Imidazoquinoxaline Src-Family Kinase p56^{Lck} Inhibitors: SAR, QSAR, and the Discovery of (*S*)-*N*-(2-Chloro-6-methylphenyl)-2-(3-methyl-1-piperazinyl)imidazo-[1,5-*a*]pyrido[3,2-*e*]pyrazin-6-amine (BMS-279700) as a Potent and Orally Active Inhibitor with Excellent in Vivo Antiinflammatory Activity

Ping Chen,* Arthur M. Doweyko,* Derek Norris, Henry H. Gu, Steven H. Spergel, Jagabundhu Das, Robert V. Moquin, James Lin, John Wityak, Edwin J. Iwanowicz, Kim W. McIntyre, David J. Shuster, Kamelia Behnia, Saeho Chong, Henry de Fex, Suhong Pang, Sydney Pitt, Ding Ren Shen, Sara Thrall, Paul Stanley, Octavian R. Kocy, Mark R. Witmer, Steven B. Kanner, Gary L. Schieven, and Joel C. Barrish

Bristol-Myers Squibb Pharmaceutical Research Institute, Princeton, New Jersey 08543-4000

Received May 7, 2003

A series of novel anilino 5-azaimidazoquinoxaline analogues possessing potent in vitro activity against p56^{Lck} and T cell proliferation have been discovered. Subsequent SAR studies led to the identification of compound **4** (BMS-279700) as an orally active lead candidate that blocks the production of proinflammatory cytokines (IL-2 and TNFα) in vivo. In addition, an expanded set of imidazoquinoxalines provided several descriptive QSAR models highlighting the influence of significant steric and electronic features. The H-bonding (Met319) contribution to observed binding affinities within a tightly congeneric series was found to be significant.

Introduction

T cell mediated immune responses play an important role in the pathogenesis of many immunological disorders, including but not limited to rheumatoid arthritis, asthma, multiple sclerosis, inflammatory bowel disease, systemic lupus erythematosus, psoriasis, and transplant rejection. Immune responses in T cells are initiated by the interaction of the T cell receptor (TCR) with an antigen bound to a glycoprotein encoded by the major histocompatibility complex (MHC). The engagement of the TCR to the antigen bound MHC is followed by a series of intracellular biochemical events, including an increase in protein tyrosine and serine/threonine phosphorylation, phospholipid hydrolysis, and changes in intracellular Ca^{2+} levels, that ultimately lead to T cell proliferation and/or differentiation. Among all the intracellular events that are required for T cell activation, the earliest and perhaps most important one is the increase in intracellular protein tyrosine phosphorylation due to the action of the nonreceptor tyrosine kinase p56^{Lck} (Lck).[1]

As one of the nine known members of the Src family of non-transmembrane protein tyrosine kinases that share a high degree of homology within their ATP-binding regions, Lck plays a critical role in the T cell receptor (TCR) signal transduction pathway.[1,2] Studies have shown that the catalytic activity of Lck is regulated by tyrosine phosphorylation at two sites: Tyr394 in the catalytic domain and Tyr505 on the C-terminus.[3] When Tyr394 is phosphorylated and Tyr505 is dephosphorylated, the fully activated enzyme can phosphorylate tyrosine residues within a special sequence called the immunoreceptor tyrosine activation motif (ITAM) located on the ζ-chain of the TCR. This phosphorylation creates a docking site for its downstream substrate ZAP-70. Subsequent phosphorylation of ZAP-70 by Lck[4,5] triggers a series of downstream cascade events that lead to mobilization of intracellular calcium (Ca^{2+})[6] and activation of protein kinase C (PKC), a serine/threonine-specific kinase.[7,8] The combination of both actions results in the activation of several nuclear transcription factors, including NF-AT and AP-1, and the transcription of their corresponding genes, ultimately leading to the generation of cytokines, such as IL-2, which drives T cell proliferation. Studies with transgenic mice have shown that T cells that lack Lck are severely impaired in TCR tyrosine phosphorylation and are unable to be activated via the TCR.[9] Because Lck expression is known to be restricted only to lymphoid cells and is required for T cell signaling,[10−13] a selective Lck inhibitor is expected to be effective and, perhaps more importantly, may offer an advantageous safety profile relative to cyclosporine A or high doses of conventional steroids for the treatment of chronic and/or acute T cell mediated autoimmune and inflammatory disorders, and for the prevention of transplant rejection.

Although knockout mice in which various Src-family kinases have been deleted display a variety of defects,[14] it has not been clearly defined in most cases whether pharmacological inhibition of Src-family kinases in adult animals would lead to similar effects, or whether at least some phenotypes observed arise primarily due to a requirement for specific Src-family kinases during discreet stages of development. For example, Lck knockout mice have been reported to display partial retinal detachment with infolding and rosette formation in the photoreceptor sheet,[15] whereas Fyn knockout mice display defects in myelination of the forebrain,[16] impaired long-term potentiation,[17] and hypersensitivity to ethanol.[18] Selective inhibitors with potent in vivo activity are required to address the question of which of the possible toxicities suggested by the phenotypes of the

* Authors to whom correspondence should be addressed. P.C.: tel (609) 252-5809; fax (609) 252-6601; e-mail ping.chen@bms.com.

10.1021/jm030217e CCC: $27.50
Published on Web 07/27/2004

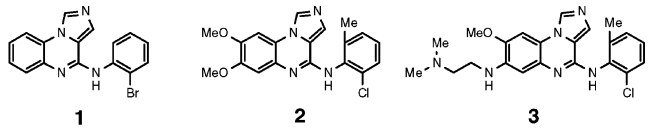

1 IC_{50} (Lck) = 170 nM, IC_{50} (T-cell) = 17 μM

2 IC_{50} (Lck) = 2 nM, IC_{50} (T-cell) = 670 nM

3 IC_{50} (Lck) = 1.7 nM, IC_{50} (T-cell) = 194 nM

Figure 1. Activity of imidazoquinoxalines **1**−**3**.

knockout mice would indeed be observed upon pharmacologic inhibition of Src-family kinases.

Several classes of Lck inhibitors, acting either at the catalytic site[19−25] or on the SH2 domains,[26−29] have been reported recently, some of which display good in vivo activity in an IL-2 production model.[24,25] Mechanistic details of enzyme inhibition may be gleaned from examination of the X-ray crystal structure of the catalytic domain of Lck in its active autophosphorylated state,[30−32] shedding light on the design of novel inhibitors. Our focus in regulating cytokine production via inhibition of T cell activation prompted us to evaluate the potential of Lck as an antiinflammatory therapeutic target. Toward this end, novel anilinoimidazoquinoxalines, represented by compound **1**, were identified as Lck inhibitors with modest potency (IC_{50} = 170 nM) from a high throughput screen of our compound collection.[33] Subsequent structural modification of **1** led to the discovery of **2**, a highly potent Lck inhibitor (IC_{50} = 2 nM) with >20-fold improvement of cellular activity against T cell proliferation over the screening hit. Unfortunately, similar to the initial hit **1**, compound **2** suffered from poor aqueous solubility (<8 μM), hampering it from further in vivo evaluation. This low aqueous solubility prompted a search for more water-soluble analogues to allow for in vivo studies. It has been reported in the literature that the addition of a "weakly basic amine tail" at either the C_6 or C_7 positions of various 4-anilinoquinazoline tyrosine kinase inhibitors resulted in improved water solubility and cellular activity.[34−37] Moreover, a closer examination of the binding model of **1**[33] revealed that the 6- and 7-positions of the fused phenyl ring point toward the open end of the ATP binding site leading toward the solvent and introduction of solubilizing groups at these positions appeared to be a viable strategy. Accordingly, incorporation of a tether that bears a polar and weakly basic tertiary amine moiety to the phenyl ring of **1** and **2** led to compounds with enhanced aqueous solubility (>100 μM) and superior in vitro and cellular activities, as demonstrated by compound **3**[38] (Figure 1).

In parallel to the above approach, we also investigated the replacement of the fused phenyl ring of **2** with various heterocycles with the objective of increasing the overall polarity of the molecule and thereby improving its aqueous solubility. In this report, we describe our effort in developing the structure−activity relationship (SAR) around the tricyclic azaimidazoquinoxaline core, which led to the discovery of compound **4** (BMS-279700), a novel, potent and orally active Lck inhibitor with excellent in vivo antiinflammatory activity (Figure 2).

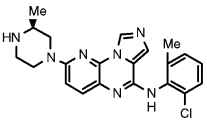

4 (**BMS-279700**)

IC_{50} (Lck) = 3.5 nM

IC_{50} (T-cell Prolif) = 273 nM

Figure 2. Activity of compound **4** (BMS-279700).

Scheme 1. Synthesis of Compound **10**[a]

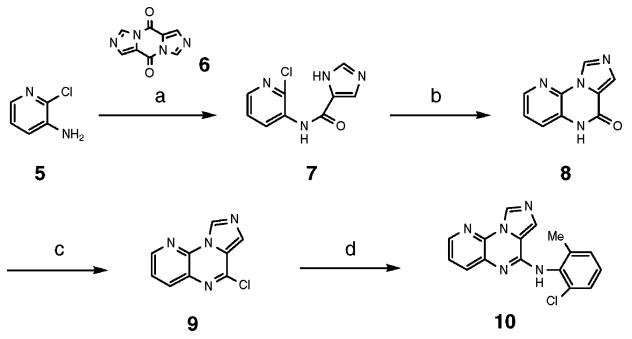

[a] (a) NaHMDS, THF, 5 h. Yield: 40%. (b) K_2CO_3, DMA, reflux, 12 h. Yield: 83%. (c) $POCl_3$, TEA, reflux, 4 h. Yield: 54%. (d) 2-Methyl-6-chloroaniline, NaHDMS, THF, rt, 2 h. Yield: 77−86%.

Scheme 2. Synthesis of Compound **4** (BMS-279700)[a]

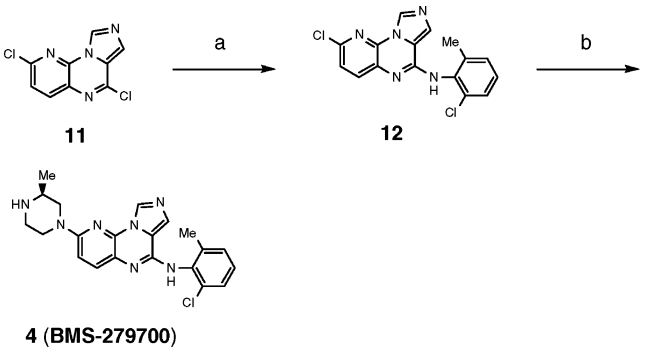

[a] (a) 2-Methyl-6-chloroaniline, NaHDMS, THF, rt, 2 h. Yield: 98%. (b) (*S*)-(+)-2-Methylpiperazine (neat), 120 °C, 5 h. Yield: 90%.

Chemistry

The anilinoimidazo[1,5-*a*]pyrido[3,2-*e*]pyrazine analogues were prepared as shown in Scheme 1 using **10** as a representative example. The construction of the tricyclic core, imidazo[1,5*a*]-pyrido[3,2-*e*]pyrazin-2-one **8**, was achieved via an intramolecular cyclization of **7** using a procedure that was developed in our laboratory.[39] Treatment of **8** with phosphorus oxychloride yielded the chloroimidate **9**, which was further coupled with 2-methyl-6-chloroaniline in the presence of a base (e.g. NaHMDS) to afford compound **10**.

Introduction of amines at the C_6 position of the anilinoimidazo[1,5*a*]pyrido[3,2-*e*]pyrazine was accomplished by a two step sequence starting from dichloride **11**, as illustrated by the synthesis of compound **4**. Reaction of **11**, prepared from 2,6-dichloro-3-aminopyridine according to Scheme 1, with 2-chloro-6-methylaniline yielded **12**, which was further reacted with (S)-3-methyl-piperazine to provide the desired compound **4**. Interestingly, the chlorine at the C_2 position is significantly more reactive than the one at the C_6 position, presumably due to the activation of the C_2 carbon by the fused imidazole ring. This difference in reactivity at the two sites allows for preferential substitution at the C_2 position, and compound **12** was obtained as the sole product (Scheme 2).

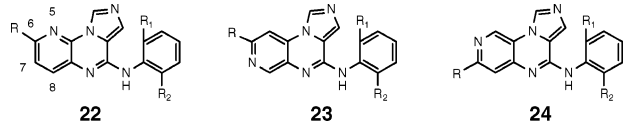

22 **23** **24**

Figure 3. Azaimidazoquinoxaline analogues **22**, **23**, and **24**.

Table 1. Inhibition of Lck (Enzyme) and T-Cell Proliferation (Human PBLs)

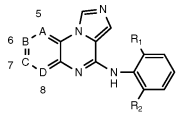

13-17

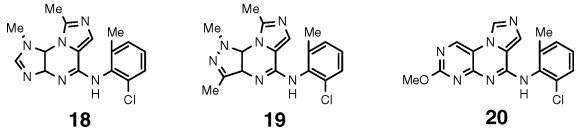

18 **19** **20**

Compd.	A, B, C, D	R_1, R_2	Lck IC_{50} (nM)[a,30]	T-cell Prolif. IC_{50} (nM)[a,31]
13	A=B=C=D=CH	2-Cl, 6-Me	9	5,000
10	A=N,B=C=D=CH	2-Cl, 6-Me	30	-
14	B=N,A=C=D=CH	2-Cl, 6-Me	1,400	-
15	C=N,A=B=D=CH	2-Cl, 6-Me	77	-
16	D=N,A=B=C=CH	2-Cl, 6-Me	90	-
17	D=N,A=B=C=CH	2, 6-di-Me	150	-
18	NA	2-Cl, 6-Me	>780	-
19	NA	2-Cl, 6-Me	>780	-
20	NA	2-Cl, 6-Me	>780	-
21	A=B=D=CH, C=C-OMe	2-Cl, 6-Me	9	2,600

[a] Average of at least three determinations (n =3).

SAR Discussion

Table 1 summarizes the structure−activity relationships for the inhibition of Lck and T cell proliferation from a series of analogues where the fused phenyl ring of compound **13** is replaced by a fused heterocycle. Incorporation of a nitrogen atom into the phenyl ring of **13**, a potent Lck inhibitor (IC_{50} = 9 nM), resulted in loss of intrinsic activity to various degrees, as illustrated by 5-aza **10** (3-fold), 6-aza **14** (>100-fold), 7-aza **15** (8-fold), and 8-aza analogues **16** and **17** (>10-fold). Replacement of the fused phenyl ring of **13** with other heterocycles, such as *N*-methyl imidazole (**18**) or *N*-methyl-C_3-methyl pyrrole (**19**), essentially abolished Lck activity, as did the 7-methoxy-6,8-pyrimidino analogue **20**. As a comparison, **20** is >80-fold less active than its carbocyclic counterpart, compound **21**. Among the analogues prepared in this series, the 5-aza analogue **10** showed the smallest reduction of activity (3-fold) from the parent carbocycle, compound **13**.

Since our earlier SAR studies indicated that substitution at the C_5 and C_8 positions of the imidazoquinoxaline core with small groups was detrimental to the activity,[33,38] we focused our attention on the SAR around the 6- and 7-positions of the fused pyridine ring of the azaimidazoquinoxalines and substituted these positions with various polar functionalities, including alcohols and amines. To this end, compounds with general structures **22**, **23**, and **24** were prepared and tested for their respective inhibitory potency (Figure 3).

Table 2. Inhibition of Lck (Enzyme) and T-Cell Proliferation (Human PBLs)

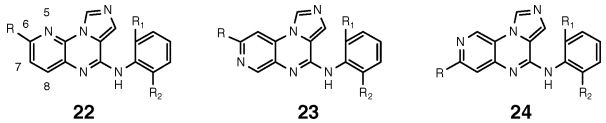

22 **23** **24**

Compd.	R	R_1, R_2	Lck IC_{50} (nM)[a,30]	T-cell Prolif. IC_{50} (nM)[a,31]
12	6-Cl	2-Cl, 6-Me	25	-
22a	6-MeO	2-Cl, 6-Me	19	1,800
22b	6-Me_2N	2-Cl, 6-Me	1	1,200
22c	6-Et_2N	2-Cl, 6-Me	2	2,100
22d		2-Cl, 6-Me	71	-
22e		2-Cl, 6-Me	5	470
22f		2-Cl, 6-Me	1	1,900
22g		2-Cl, 6-Me	7	-
22h		2, 6-di-Me	1	230
22i		2-Cl, 6-Me	1	400
22j		2-Cl, 6-Me	6	540
22k		2-Cl, 6-Me	2	400
23		2-Cl, 6-Me	29	-
24a		2-Cl, 6-Me	163	-
24b		2-Cl, 6-Me	240	-
24c		2-Cl, 6-Me	103	-

[a] Average of three determinations (n =3). [b] For comparison, CsA has an IC_{50} = 115 nM against T cell proliferation in the same assay.

Substitution at the C_6 position of **10** with a chloro (**12**) or methoxy (**22a**) group had a minimal effect on potency (Table 2). Interestingly, incorporation of a small amino group at this position led to a significant increase in intrinsic potency, as demonstrated by compounds **22b** (30-fold) and **22c** (15-fold). Unfortunately, this favorable increase in potency did not translate into an improvement in cellular activity. Compounds **22b** and **22c** are essentially equipotent to **22a** in a T cell proliferation assay and are only slightly better than the parent carbocycle, compound **13**. In addition, introduction of a polar *N*,*N*-dimethylaminoethylamino tether at the C_6

position of **10** led to a significant loss of enzyme activity (**22d**). Incorporation of a small heteroaromatic group (e.g. imidazole) at this position led to not only a gain in intrinsic potency but also an improvement in cellular activity (**22e**). Further investigation using sterically bulky secondary amines led to some interesting results. While the morpholinyl (**22f**) and piperidinyl (**22g**) analogues showed minimal improvement in enzyme and cellular activities in comparison to the diethylamino analogue **22c**, compounds with heterocycles bearing an additional basic nitrogen (**22h**−**k**) all displayed markedly enhanced cellular activity. Compound **22h** is a highly active Lck inhibitor that displays potent cellular activity in blocking T cell proliferation (IC_{50} = 230 nM) (Table 2). It is conceivable that such an improvement in cellular activity is most likely due to an improvement in aqueous solubility as well as an enhancement in cell permeability, a trend observed by other known PTK inhibitors in the literature.[34−37] Surprisingly, an analogue with an aliphatic tether possessing a basic nitrogen was significantly less potent (>70-fold) than its heterocyclic counterpart (**22d** vs **22h**), highlighting the necessity for the conformational constraint imposed by a heterocycle at this position (vide infra).

Substitutions at the C_6 position of **23** and C_7 position of **24** were also investigated (Table 2). In general, within the C_6-substituted series (i.e. **22** and **23**), the 5-aza analogues are consistently more potent than the 7-aza analogues, as demonstrated by the activities of **22k** and **23** (>10-fold).[40] In addition, analogues derived from the C_7-substituted 6-aza scaffold **24** are significantly less active, all of which displayed IC_{50} of greater than 100 nM (**24a**−**c**).

Encouraged by the significant improvement in cellular activity by **22h**, our attention focused on the 5-aza series and substitution by various heterocycles at the C_6 position. The in vitro biological data from these studies are summarized in Table 3.

Analogues with substituted pyrrolidine moieties (**25**−**30**) showed similar enzyme and cellular potency in comparison to **22h**, with the exception of diol **28**, which displayed diminished potency in inhibiting T cell proliferation. On the other hand, all piperazine analogues (**4**, **22h**, and **31**−**36**) were consistently among the most potent Lck inhibitors, both against the enzyme and in blocking T cell proliferation. Unlike the *N*,*N*-dimethylaminoethylamino analogue **22d** of Table 2, analogues bearing open-chained amino alcohol groups were potent Lck inhibitors with good (**37**) to modest (**36**, **38**−**40**) cellular activity. However, due to the lack of a basic amine moiety, these analogues suffered from reduced solubility when compared with the piperazine analogues, such as **4**, **32**, and **33** (Table 3).

Compound **4** was further profiled against a panel of protein kinases for selectivity, and the results are shown in Table 4. In general, compound **4** is highly selective (>1000−10000-fold selectivity) vs kinases from other families of serine/threonine (with the exception of p38, a MAP kinase, where a 95-fold selectivity was observed) and tyrosine kinases. Notably, it is significantly less selective or nonselective in comparison to kinases within the Src family.

Table 3. Inhibition of Lck (Enzyme) and T-Cell Proliferation (Human PBLs)

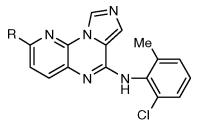

25-40

Compd.	R	Lck IC_{50} (nM)[a,30]	T-cell Prolif. IC_{50} (nM)[a,31]	Solubility (mg/mL)[b]
25		4	340	
26		8	730	
27		5	440	12.5-25
28		13	>2,000	
29		6	370	
30		7	310	
4 (**BMS-279700**)		**4**[c]	**165**	**>100**
31		2	240	
32		5	270	75
33		3	180	70
34	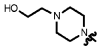	9	240	22-28
35	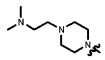	2	250	
36		4	620	17
37		7	300	14.5-25
38		13	630	
39		3	620	20
40		3	490	<12.5

[a] Average of three determinations (n =3). [b] Solubility in PG/EtOH/IPM (50:45:5). [c] K_i (Lck) = 0.55 ± 0.04 nM, K_d (Lck) = 0.17 ± 0.03 nM (n = 3).

Table 4. Selectivity Profile of Compound **4** (BMS-279700)

kinase	IC_{50} (nM)	kinase	IC_{50} (nM)
Syk	>10000	Lck	4
ZAP-70	>1000	Src	4
PKA	>10000	Fyn	5
PKC	>10000	Lyn	0.5
CDK	>10000	Fgr	2.8
IKK1,2	>10000	Yes	4.7
HER1,2	>1000	Hck	23
PDGF−R	>1000	Blk	27
VEGF−R	>1000	p38	380

In addition to the measurement of cellular activity by the inhibition of T cell proliferation, inhibitory effects on production of inflammatory cytokines, such as IL-2,

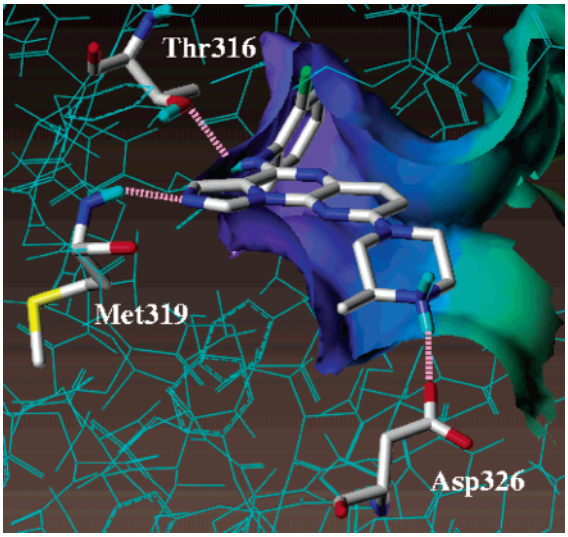

Figure 4. Inhibitor **22h** (protonated at piperazine NH) modeled into the ATP-binding site of Lck illustrating key interactions between the ligand and binding site: (1) deep hydrophobic pocket occupied by the angular di-ortho-substituted aniline ring, (2) hydrogen bond between Thr316 and aniline NH, and (3) hydrogen bond between Met319 and imidazolyl N, and (4) a putative electrostatic interaction between protonated piperazine and Asp326.

Table 5. Solubility of 5-Azaimidazoquinoxaline Analogue **4** (Free Base and HCl Salt)

compd	water (mg/mL)
4 (BMS-279700)	0.003
4·HCl	9.2

by the 5-azaimidazoquinoxaline analogues were also examined. In T cells, compound **4** displayed potent inhibitory activity against IL-2 production (IC_{50} = 200 nM) when challenged by anti-CD3/anti-CD28 costimulation. This is consistent with the mechanism of action of an Lck inhibitor since inhibition of Lck blocks TCR signaling, resulting in the reduction of IL-2 production and, ultimately, leading to T cell inactivation. Interestingly, compound **4** also inhibits LPS-induced tumor necrosis factor α (TNFα) production in human PBLs (IC_{50} = 295 nM). This inhibition of TNFα may be due to its ability to inhibit the Src-family kinases expressed in monocytes. LPS has been reported to activate the Src-family kinases Hck, Fgr, and Lyn in monocytes,[41] and manipulation of levels of active Hck in a murine macrophage cell line and in transgenic mice indicates that Hck can regulate LPS-induced TNFα production in murine macrophages.[42,43] Inhibition of p38 kinase may also potentially contribute to the inhibition of TNFα production by the compound.

The aqueous solubility of compound **4** was determined. As expected, in water, the HCl salt of compound **4** is significantly more soluble than the free base (Table 5).

The enhancement (>10-fold) of intrinsic potency displayed by C_6-substituted 5-aza analogues, represented by **4** and **22h**, over the nonsubstituted 5-aza analogue **10** is consistent with our proposed binding model established using the published coordinates of an activated Lck kinase domain bound to ANP (a nonhydrolyzable ATP mimic). Figure 4 illustrates the proposed binding mode of compound **22h** in the ATP pocket of Lck. Favorable hydrophobic interactions between the 2,6-disubstituted aniline moiety (which adopts a preferred out-of-plane orientation in comparison to the tricyclic system) and the angular hydrophobic pocket of the enzyme are likely. In addition, two critical hydrogen bonding interactions (N_3-nitrogen of imidazole to the NH of Met319 and the NH of the aniline to the OH of Thr316) appear to be probable. This hydrogen-bonding motif is common to this class of inhibitors. Perhaps equally important is the presence of a third ionic hydrogen-bonding interaction between the NH of the piperazine of **22h** and the carboxylate of Asp326, which may play a significant role in the enhancement in the binding affinity of these analogues (Figure 4).

On the basis of its promising in vitro and cellular activities, compound **4** was further evaluated in vivo. The pharmacokinetic properties of **4** were obtained from studies in mice, rats, and dogs following intravenous and oral administration (Table 6). In general, compound **4** had a more favorable phamacokinetic profile in dogs than in rodents. For example, in mice and rats, compound **4** displayed a higher clearance rate (86 and 109 mL/min/kg, respectively) and a relatively short half-life (3.2 and 2.4 h, respectively). This trend is also reflected in the observed order of oral bioavailabilities in three species (19%, 20%, and 77%, respectively). In addition, compound **4** has a favorable protein binding profile: 91.12% (±0.81) for mouse and 84.82% (±1.41) for human, indicating that a relatively high free fraction can be achieved upon in vivo dosing.

To evaluate the in vivo efficacy of the 5-azaimidazoquinoxaline chemotype, compound **4** was tested in a mouse anti-CD3-stimulated IL-2 production model. In this model, compound **4** displayed a 50% reduction of serum IL-2 when dosed orally at 20 mpk (data not shown). At 50 mpk, a 78% reduction of serum IL-2 levels was achieved (Figure 5).

As one of the major proinflammatory cytokines, TNFα plays a critical role in both acute and chronic inflammatory responses and is often implicated in various

Table 6. Pharmacokinetic Properties of Compound **4** (BMS-279700)

	mouse (n = 3)		rat (n = 3)		dog (n = 2)	
	iv dose	po dose	iv dose	po dose	iv dose	po dose
dose[a] (mg/kg)	10	10	10	10	10	10
AUC-iv (μM h)	4.75 ± 0.36		3.75 ± 0.18		9.97 ± 1.16	
Vss (L/kg)	14.5 ± 1.4		21 ± 1		22 ± 3	
Cl (mL/min/kg)	86 ± 6		109 ± 5		41 ± 5	
$t_{1/2}$ (h)	3.2 ± 1.4		2.4 ± 0.1		6 ± 1	
AUC-po (μM h)		0.90 ± 0.17		0.62 ± 0.28		6.84 ± 2.69
MRT (h)		6.1 ± 1.4		4.1 ± 0.2		9 ± 1
F (%)		19		20		77

[a] Compound **4** was dosed as a solution in PEG300:water (3:1).

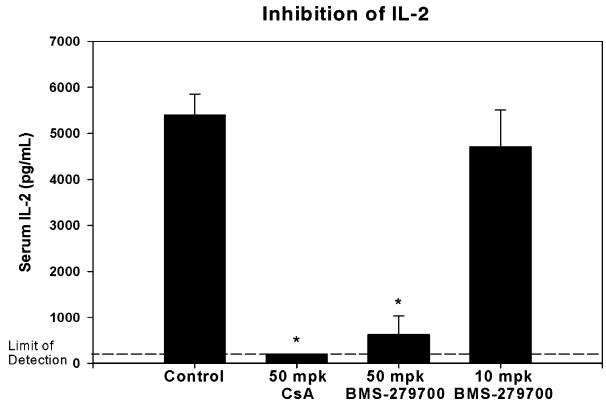

Figure 5. Inhibition of anti-CD3/anti-CD28-induced IL-2 production in mouse by compound **4** (BMS-279700).

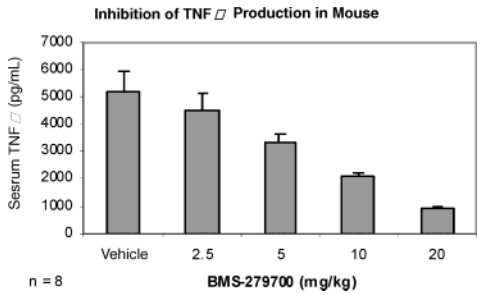

Figure 6. Inhibition of LPS-induced TNF-α production in mouse. Compound **4** (BMS-279700) was dosed orally.

inflammatory autoimmune diseases.[44−51] Studies have shown that treatment of RA patients with monoclonal antibodies or soluble TNF receptor to antagonize TNFα resulted in significant clinical efficacy.[52−57] The promising clinical data from anti-TNFα biologics led to FDA approval of Enbrel (Etanercept), Remicade, and Humira as antiarthritic therapies. In addition, small molecule drugs that inhibit the formation of TNFα have also been disclosed recently.[58] Since compound **4** displayed in vitro activity against LPS-induced TNFα production in human PBLs (vide supra), it was further tested in a mouse LPS-induced TNFα production model for in vivo efficacy. Consistent with the in vitro result, compound **4** suppressed serum TNFα production in mice in a dose-dependent fashion (Figure 6), demonstrating that compound **4** could be potentially useful as an oral agent in treating inflammatory diseases associated with elevated TNFα levels.

Modeling

In an effort to ascertain the structural and/or molecular properties associated with potent inhibition, quantitative structure−affinity correlations were determined for selected members of the imidazoquinoxaline series using several multiple linear regression approaches wherein classical Hansch descriptors served to highlight significant structural/electronic features potentially correlated with observed Lck binding affinity. In addition, it was of interest to examine the possibly significant role of hydrogen bonding between the ligand imidazolyl N and backbone NH (Met319).

Some structural details of kinase inhibitor binding have been published which provided the basis for the construction of an Lck binding site model illustrated in Figure 7.[30−32] This model of the catalytic domain is

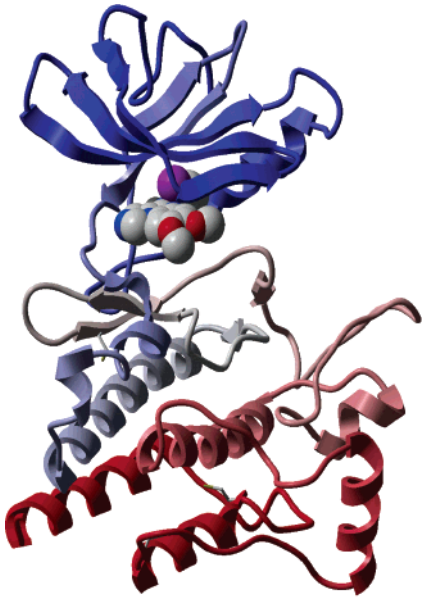

Figure 7. Lck model derived from published structures[25−27] and homology modeling based on the Hck structure.[4] Compound **2** was docked into the ATP binding site.

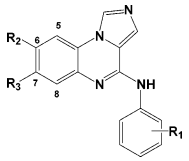

Figure 8. Imidazoquinoxaline scaffold used in QSAR analyses 1 (R_1 = di-ortho substituted, $R_2 = R_3 = H$) and 2 (R_1 = mono-, di-, and trisubstituted; R_2 = H, OCH_3; R_3 = H, OCH_3).

based on the active, autophosphorylated form of Lck. Inspection of the inhibitor binding motif suggested several possibly critical interactions, namely, (1) a deep pocket, hydrophobic interaction involving the pendant di-ortho-substituted aniline ring; (2) a hydrogen bond between Thr316 OH (acceptor) and the anilino NH (donor); and (3) a hydrogen bond between Met319 backbone NH (donor) and the imidazolyl N (acceptor). These interactions were considered critical to the overall activity of the imidazoquinoxaline series (as illustrated in Figure 4).

Modeling Discussion

Two QSAR analyses were conducted in order to ascertain the relative contributions of key features within the imidazoquinoxaline series. The descriptor sets included typical Hansch parameters (F, R, π, MR, and V_m = molecular volume) along with indicator variables as appropriate. The first analysis was limited to those compounds containing ortho-disubstituted anilines (R_1, Figure 8, where $R_2 = R_3 = H$) and comprised a total of 19 analogues with an IC_{50} range[33] of 9 nM to 12.5 μM. Two equations (eqs 1, 2) emerged with modest correlation (r^2 = 0.65−0.68) which were statistically indistinguishable. While both indicated a negative effect on binding affinity due to large ortho substitutents (MR_o), eq 1 suggests that the mathematical counterpoint comes from positive effects due to the electron-withdrawing nature of such groups (F, R), whereas eq 2 achieves an equivalent result with hydrophobicity (π).

QSAR Analysis 1.

$$pIC_{50} = -0.95\ MR_o + 0.65\ F + 2.62\ R + 3.16 \quad (1)$$

$$r^2 = 0.65 \qquad F = 9.24 \qquad s = 0.61 \qquad N = 19$$

$$pIC_{50} = -0.92\ MR_o + 1.75\ \pi^2 - 0.43\ \pi + 0.862 \quad (2)$$

$$r^2 = 0.68 \qquad F = 10.8 \qquad s = 0.58 \qquad N = 19$$

A second QSAR analysis focused on an expanded set of imidazoquinoxalines ($N = 114$, IC_{50} range of 1 nM to 12.5 μM), wherein mono-, di-, and trisubstituted anilines (Figure 8, R_1) were included, along with OCH_3 substituents at positions 6 and 7 (Figure 8, R_2, R_3). The descriptor set was augmented with indicator variables accounting for specific substitution patterns, e.g., oMe = *o*-methyl aniline. A step-up multiple linear regression approach yielded a series of plausible equations (eqs 3−7, all correlated with pIC_{50} ($pIC_{50} = -\log IC_{50}$)). Values in parentheses refer to positions on the aniline ring. Bolded descriptors are newly added in the step-up regression analysis sequence.

QSAR Analysis 2.

$$+1.37\ F(2) + 1.66\ \pi(6) - 0.14\ MR(6) + 2.81\ F(6) + 1.82\ oMe - 0.69 \quad (3)$$

$$r^2 = 0.65 \qquad r(cv)^2 = 0.60 \qquad F = 39.4$$

$$+1.34\ F(2) + 1.96\ \pi(6) - 0.13\ MR(6) + 2.46\ F(6) + 1.83\ oMe - \mathbf{0.01\ Vm} - 0.20 \quad (4)$$

$$r^2 = 0.69 \qquad r(cv)^2 = 0.64 \qquad F = 39.2$$

$$-1.17\ F(3) + 0.66\ \pi(6) + 2.67\ F(6) + 1.59\ oMe - 0.01\ Vm + \mathbf{0.80\ oCl} - 0.07 \quad (5)$$

$$r^2 = 0.71 \qquad r(cv)^2 = 0.66 \qquad F = 43.3$$

$$-1.17\ F(3) + 0.64\ \pi(6) + 1.53\ F(6) + 1.35\ oMe - 0.01\ Vm + 0.62\ oCl + \mathbf{0.80\ diMeO} + 0.06 \quad (6)$$

$$r^2 = 0.75 \qquad r(cv)^2 = 0.71 \qquad F = 45.4$$

$$+ 0.39\ \pi(2) - 0.91\ R(4) + 0.96\ oMe - 0.02\ Vm + 0.64\ oCl + 0.71\ diMeO + \mathbf{0.94\ diOrtho} - 0.20 \quad (7)$$

$$r^2 = 0.76 \qquad r(cv)^2 = 0.71 \qquad F = 46.7$$

QSAR analysis 2 clearly points out the significant contributions to activity brought about by specific substituents, namely, the presence of a OCH_3 at positions 6 and 7 (diMeO), the di-ortho substitution (diOrtho), the *o*-methyl and *o*-chloro (oMe and oCl, respectively). These indicator variables are set to 1 when the group is present and 0 when absent. The ortho-substitution effect is consistent with the proposed binding model, since such substitution of the aniline would place the ring into the out-of-plane conformation required for the aniline ring to enter the deep hydrophobic pocket. The apparent preference for an *o*-chloro and *o*-methyl pattern is consistent with QSAR analysis 1, wherein these two moieties are among the set of di-ortho substituents calculated to have an optimum size and electronic property according to eq 1.

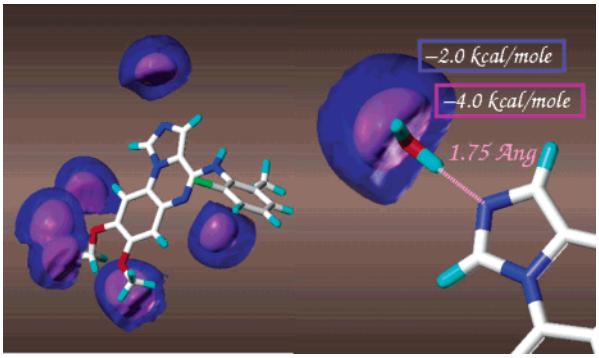

Figure 9. Hydrogen bond donor locations are illustrated herein as determined using a grid-based analysis.[10] Compound **2** is shown with contours (outer −2.0 kcal/mol; inner −4.0 kcal/mol) developed using an NH_3^+ probe at a grid spacing of 0.25 Å. The upper left contour represents the location for water in the SAM1 hydrogen bond modeling procedure.

Table 7. Imidazoquinoxaline Hydrogen-Bonding Analysis Data Set (Hydrogen Bond Enthalpies, HB H_f, Determined Using SAM1)

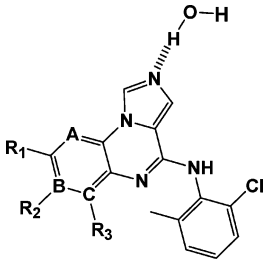

compound	R_1	R_2	R_3	A	B	C	pIC_{50} (μM)	HB H_f (kcal/mol)
22b	$N(CH_3)_2$	H		N			3.00	−3.56
2	OCH_3	OCH_3					2.70	−3.60
21	OCH_3	H					2.52	−3.44
	Ph	H					2.22	−3.39
	NH_2	H					2.15	−3.45
	H	OCH_3					2.06	−3.50
	H	H					2.05	−3.33
	H	$COOCH_3$					1.85	−3.27
	NO_2	H					1.80	−3.17
	Cl	Cl					1.69	−2.90
	H	NH_2					1.68	−3.50
12	Cl	H		N			1.60	−3.09
	F	H					1.59	−3.14
	H	Cl					1.52	−3.33
10	H	H		N			1.52	−3.12
15	H	H			N		1.11	−3.16
	F	H	Br				1.10	−2.98
16	H	H				N	1.05	−3.23

The possibility that 6,7-di-OCH_3 substitution yielded congeners with enhanced Lck binding affinities because of a modulating effect on the proposed hydrogen bond between imidazolyl N and Met319 was examined next. In order to explore the possible correlation of hydrogen bond strength to observed binding, we needed a model method to estimate the hydrogen bond enthalpy between a water molecule acting as donor and a heteroatom (imidazolyl N) acting as an acceptor. To this end, the semiempirical method, SAM1,[61] was used to geometry optimize a modeled system consisting of the imidazoquinoxaline core and water (see Figure 9 and Table 7), affording an estimate for the enthalpies of complexed and free species. The differences provided the hydrogen

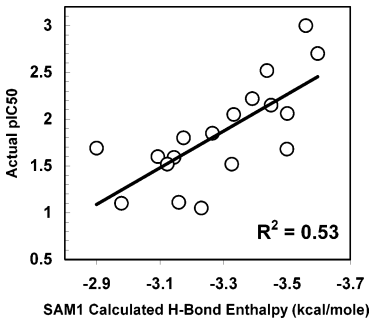

Figure 10. Correlation of observed Lck binding affinities (actual pIC50) with SAM1 calculated hydrogen bond enthalpies.

bond enthalpy between water and the imidazoquinoxaline (the enthalpy, H_f, for water was determined as −57.04 kcal/mol and was used as a constant in these calculations).

The 18 imidazoquinoxalines of Table 7 were selected on the basis of their orientations in the Lck binding site model, with care being taken to limit the selection to those molecules with relatively small R_1/R_2 groups in order to avoid additional obfuscating interactions with the site. SAM1[59] estimates of hydrogen bond enthalpies appeared to correlate well with observed Lck binding affinities ($r^2 = 0.53$), especially when considering the underlying assumption that no other significant interactions were introduced in this series. These comparisons are given in Table 7 and illustrated in Figure 10.

The observation of a significant correlation between hydrogen bonding in a series of kinase inhibitors and their observed binding affinities is not without precedence. Such an inference was made in the case of pyridyl-containing p38 kinase inhibitors wherein the relationship focused on the electrostatic potential at the pyridyl nitrogen,[60,61] and for a series of flavonoid inhibitors of $p56^{Lck}$ where a quantum chemical parameter set defining hydrogen bonding was correlated with activity.[62] Interestingly, in a study aimed at defining the determinants of ligand binding to cAMP-dependent protein kinase, theoretical models based on continuum electrostatics and surface area dependent nonpolar terms suggested that hydrogen bonding represents a negligible contribution to binding.[63] In contrast, the present study clearly demonstrates a non-negligible contribution to binding. It would appear that further investigation into the role of hydrogen bonding in protein−ligand interactions may provide some needed illumination and that generalizations regarding the secondary role of intermolecular hydrogen bonds in binding sites may be premature.

Conclusions

A series of novel anilino 5-azaimidazoquinoxaline analogues possessing potent in vitro inhibitory activity against $p56^{Lck}$ have been identified. Incorporation of polar, small heterocycles at the C_6 position of the 5-azaimidazoquinoxaline tricyclic scaffold led to compounds with enhanced intrinsic potency as well as improved activities in blocking human T cell proliferation. These modifications resulted in enhanced physicochemical properties for this class of compounds. From this series, compound **4** (**BMS-279700**) was identified as the lead candidate and was shown to be orally active with excellent in vivo antiinflammatory efficacy in mice (inhibition of IL-2 and TNFα). Compound **4** and the other members of this series should be of value to help define the benefits of Src-family kinase inhibition in animal models of disease, as well as to investigate possible toxicities that may arise from inhibition of these kinases. In addition, using tools of molecular modeling, the structural factors underlying $p56^{Lck}$ binding affinity were identified. Multiple regression analysis (QSAR) highlighted the importance of the di-ortho-substituted aniline and the use of small, electron-withdrawing substituents to ensure an out-of-plane ring orientation and best fit for the deep, hydrophobic pocket of $p56^{Lck}$. Furthermore, a significant role of the putative hydrogen bond between inhibitor (imidazolyl N) and protein (Met319, NH) was proposed on the basis of the correlation observed between calculated H-bond enthalpies and binding affinities for a selected set of imidazoquinoxalines.

Experimental Section

Chemistry. All solvents and reagents were obtained from commercial sources and used without further purification unless indicated otherwise. Melting points were obtained from a Mel-Temp 3.0 or Fisher-Johns melting point apparatus and are uncorrected. ^{1}H NMR and ^{13}C NMR spectra were obtained on a JEOL 400 MHz CPF-270 spectrometer operating at 270 or 67.5 MHz, respectively, and chemical shifts are reported in parts per million (δ) from the tetramethysilane resonance in the indicated solvent. High-resolution mass spectra were taken with a Micromass LCT spectrometer using ESI-TDF ionization. All new compounds were homogeneous by thin-layer chromatography (TLC) and reversed-phase HPLC (>98%). Flash chromatography was carried out on E. Merck Kieselgel 60 silica gel (230−400 mesh). Preparative HPLC was performed on a YMC OD S-10 50 × 500 mm column eluting with a mixture of solvents A and B using a gradient elusion (solvent A, 10% MeOH−90% H_2O−0.1% TFA; solvent B, 90% MeOH−10% H_2O−0.1% TFA; UV 254 or 210 nm). Analytical HPLC was performed on a YMC OD S-5 4.6 × 50 mm column eluting with a mixture of solvents A and B using a gradient elution (solvent A, 10% MeOH−90% H_2O−0.1% TFA; solvent B, 90% MeOH−10% H_2O−0.1% TFA; UV 254 or 210 nm).

***N*-(2-Chloro-3-pyridinyl)-1*H*-imidazole-4-carboxamide (7).** To 3-amino-2-chloropyridine (2.87 g, 22.3 mmol) in THF (13 mL), cooled in a −10 °C bath, was added sodium bis(trimethylsilyl)amide (51 mL, 51.0 mmol, 1.0 M in THF). The mixture was stirred for 1 h, and a suspension of imidazole carbonyl dimer[39] (2 g, 10.6 mmol) in THF (20 mL) was added and let warm to room temperature. The mixture was stirred for 2 h, and acetic acid was added. The reaction mixture was concentrated in vacuo followed by the addition of water and saturated sodium bicarbonate. The solid was collected by filtration, washed by water and hexane, and dried under high vacuum to give **7** as a light beige solid (Yield: 40%). ^{1}H NMR (400 MHz, $CDCl_3$): δ 12.13 (bs, 1H), 9.65 (s, 1H), 8.93 (dd, J = 1.71 Hz, J = 8.12 Hz, 1H), 8.09 (dd, J = 1.71 Hz, J = 4.49 Hz, 1H), 7.74 (s, 1H), 7.63 (s, 1H), 7.29 (dd, J = 4.49 Hz, J = 8.12 Hz, 1H).

Imidazo[1,5-*a*]pyrido[3,2-*e*]pyrazine-6(5*H*)-one (8). A mixture of **7** (1.89 g, 8.49 mmol) and potassium carbonate (3.5 g, 25.5 mmol) in dimethylacetamide (40 mL) was heated to reflux for 6 h. The reaction mixture was then concentrated in vacuo followed by the addition of water and saturated ammonium chloride. The solid was collected by filtration, washed with water, and dried under high vacuum to give **8** as a light beige solid (Yield: 83%). Mp: 295−300 °C. ^{1}H NMR (400 MHz, DMSO-d_6): δ 11.49 (s, 1H), 8.88 (s, 1H), 8.23 (dd, J = 1.37 Hz, J = 4.69 Hz, 1H), 7.89 (s, 1H), 7.67 (dd, J = 1.37, J = 8.06, 1H), 7.45 (dd, J = 4.57, J = 8.06, 1H). MS (ESI): m/z = 187 (M + 1). HR-MS (FAB) for $C_9H_7N_4O$ (MH^+): calcd 187.0620, found 187.0650.

6-Chloroimidazo[1,5-*a*]pyrido[3,2-*e*]pyrazine (9). To **8** (1.37 g, 7.36 mmol) was added phosphorus oxychloride (20 mL), and the mixture was heated to reflux for 12 h. The reaction mixture was concentrated in vacuo, and the residue was cooled in an ice bath. Water was added to the residue and neutralized with saturated sodium bicarbonate. The solid was collected by filtration and purified using flash column chromatography on silica gel to yield **9** as a light yellow solid (Yield: 54%). Mp: 194−195 °C. ^{1}H NMR (400 MHz, DMSO-d_6): δ 9.28 (s, 1H), 8.70 (dd, J = 4.70 Hz, J = 1.48 Hz, 1H), 8.36 (dd, J = 1.48 Hz, J = 8.10 Hz, 1H), 8.07 (s, 1H), 7.74 (dd, J = 4.70 Hz, J = 8.10 Hz, 1H). MS (ESI): m/z = 205 (M + 1). HR-MS (ESI-TDF) for $C_9H_6ClN_4$ (MH^+): calcd 205.0281, found 205.0278.

***N*-(2-Chloro-6-methyphenyl)imidazo[1,5*a*]pyrido[3,2-*e*]pyrazin-6-amine (10).** To a solution of 2-chloro-6-methylaniline (12.5 mg, 0.088 mmol) in THF (0.4 mL) was added a solution of sodium bis(trimethylsilyl)amide (0.22 mL, 0.22 mmol, 1.0 M in THF), and the reaction mixture was heated to reflux for 0.5 h. The reaction mixture was cooled to room temperature,and compound **9** (18 mg, 0.088 mmol) in THF (0.8 mL) was added. The mixture was again heated to reflux for 0.5 h and then cooled to room temperature and quenched with acetic acid. The reaction mixture was concentrated in vacuo followed by addition of water and saturated sodium bicarbonate. The solid was collected by filtration, washed with water and hexane, and dried under high vacuum to give 23.4 mg of **10** as a pale yellow solid (Yield: 86%). Mp: 189−192 °C. ^{1}H NMR (400 MHz, DMSO-d_6): δ 9.89 (bs, 1H), 9.30 (s, 1H), 8.72 (dd, J = 4.70 Hz, J = 1.48 Hz, 1H), 8.40 (dd, J = 1.48 Hz, J = 8.10 Hz, 1H), 8.07 (s, 1H), 7.74 (dd, J = 4.70 Hz, J = 8.10 Hz, 1H), 7.25−7.43 (m, 3H), 2.25 (s, 3H). MS (ESI): m/z = 310 (M + 1). HR-MS (ESI-TDF) for $C_{16}H_{12}ClN_5$ (MH^+): calcd 310.0789, found 310.0792.

2,6-Dichloroimidazo[1,5-*a*]pyrido[3,2-*e*]pyrazine (11). Compound **11** was prepared from 2,6-dichloro-3-amino-pyridine using a method analogous to the preparation of **9**. ^{1}H NMR (400 MHz, DMSO-d_6): δ 9.25 (s, 1H), 8.39 (d, J = 8.56 Hz, 1H), 8.09 (s, 1H), 7.81 (d, J = 8.56 Hz, 1H).

2-Chloro-*N*-(2-chloro-6-methyl-phenyl)imidazo[1,5-*a*]-pyrido[3,2-*e*]pyrazin-6-amine (12). Compound **12** was prepared from **11** (142 mg, 0.59 mmol), 2-chloro-6-methylaniline (0.073 mL, 0.59 mmol), and sodium bis(trimethylsilyl)amide (1.43 mL, 1.43 mmol, 1.0 M solution) in THF (10 mL) using a method analogous to the preparation of **10** (Yield: 98%). Mp: 185−187 °C. ^{1}H NMR (400 MHz, DMSO-d_6): δ 9.90 (bs, 1H), 8.96 (s, 1H), 8.18 (m 1H), 7.76 (d, J = 8.32 Hz, 1H), 7.33−7.45 (m, 2H), 7.24−7.31 (m, 2H), 2.23 (s, 3H).

(*S*)-*N*-(2-Chloro-6-methylphenyl)-2-[3-methyl-1-piperazinyl)imidazo[1,5-*a*]pyrido[3,2-*e*]pyrazin-6-amine (4) (= BMS-279700, Free Base). The mixture of compound **12** (300 mg, 0.87 mmol) and (*S*)-3-methyl-1-piperazine (5 mL) was heated to 120 °C for 5 h. After cooling to room temperature, water and saturated sodium bicarbonate were added. The solid was collected by filtration, washed with water and hexane, and dried under high vacuum to give **4** as an off-white solid (Yield: 90%). Mp: 165−168 °C. ^{1}H NMR (400 MHz, DMSO-d_6): δ 9.00 (bs, 1H), 8.87 (s, 1H), 7.89 (bs, 1H), 7.52 (d, J = 8.98 Hz, 1H), 7.36 (dd, J = 1.22 Hz, 1H), 7.18−7.26 (m, 2H), 6.83 (d, J = 8.98 Hz, 1H), 4.17 (m, 2H), 2.90 (m, 1H), 2.58−2.75 (m, 3H), 2.34 (m, 1H), 2.22 (m, 1H), 2.17 (s, 1H), 0.99 (d, J = 6.26 Hz, 3H). MS (ESI): m/z = 408$^+$ (M + 1). HR-MS (ESI-TDF) for $C_{21}H_{22}ClN_7$ (MH^+): calcd 408.1703, found 408.1710.

***N*-(2-Chloro-6-methylphenyl)imidazo[1,5-*a*]pyrido[4,3-*e*]pyrazine-4-amine (14).** Compound **14** was prepared from imidazo[1,5-*a*]pyrido[4,3-*e*]pyrazine-6(5*H*)-one[64] using a method analogous to the preparation of **10**. Mp: 200−202 °C. ^{1}H NMR (400 MHz, DMSO-d_6): δ 9.90 (s, 1H), 9.46 (s, 1H), 9.31 (s, 1H), 8.37 (d, J = 5.26 Hz, 1H), 8.23 (s, 1H), 7.23−7.55 (m, 4H), 2.25 (s, 3H). MS (ESI): m/z = 310$^+$ (M + 1). HR-MS (ESI-TDF) for $C_{16}H_{13}ClN_5$ (MH^+): calcd 310.0859, found 310.0865.

***N*-(2-Chloro-6-methylphenyl)imidazo[1,5-*a*]pyrido[3,4-*e*]pyrazine-4-amine (15).** Compound **15** was prepared from imidazo[1,5-*a*]pyrido[3,4-*e*]pyrazine-6(5*H*)-one[64] using a method analogous to the preparation of **10**. ^{1}H NMR (400 MHz, $CDCl_3$): δ 8.91 (bs, 1H), 8.64 (s, 1H), 8.49 (d, J = 5.33 Hz, 1H), 7.66 (d, J = 5.33 Hz, 1H), 7.39 (m, 1H), 7.25−7.35 (m, 3H), 6.80 (bs, 1H), 2.36 (s, 3H). MS (ESI): m/z = 310$^+$ (M^+ + 1). HR-MS (ESI-TDF) for $C_{16}H_{13}ClN_5$ (M^+ + H): calcd 310.0859, found 310.0852.

***N*-(2-Chloro-6-methylphenyl)imidazo[1,5-*a*]pyrido[2,3-*e*]pyrazine-4-amine (16).** Compound **16** was prepared from imidazo[1,5-*a*]pyrido[2,3-*e*]pyrazine-6(5*H*)-one[64] using a method analogous to the preparation of **10**. ^{1}H NMR (400 MHz, DMSO-d_6): δ 9.08 (bs, 1H), 8.59 (d, J = 8.12 Hz, 1H), 8.36 (d, J = 4.27 Hz, 1H), 7.89 (bs, 1H), 7.35−7.40 (m, 1H), 7.33 (dd, J = 8.12 Hz, J = 4.27 Hz, 1H), 7.17−7.28 (m, 2H), 2.30 (s, 3H). MS (ESI): m/z = 310$^+$ (M + 1). HR-MS (ESI-TDF) for $C_{16}H_{13}ClN_5$ (MH^+): calcd 310.0859, found 310.0848.

***N*-(2,6-Dimethylphenyl)imidazo[1,5-*a*]pyrido[2,3-*e*]pyrazine-4-amine (17).** Compound **17** was prepared from imidazo[1,5-*a*]pyrido[2,3-*e*]pyrazine-6(5*H*)-one[64] using a method analogous to the preparation of **10**. ^{1}H NMR (400 MHz, DMSO-d_6): δ 9.10 (bs, 1H), 8.60 (d, J = 8.12 Hz, 1H), 8.42 (d, J = 4.30 Hz, 1H), 7.89 (bs, 1H), 7.35−7.40 (m, 1H), 7.33 (dd, J = 8.12 Hz, J = 4.30 Hz, 1H), 7.19−7.29 (m, 2H), 2.32 (s, 6H). MS (ESI): m/z = 290$^+$ (M + 1). HR-MS (ESI-TDF) for $C_{17}H_{16}N_5$ (MH^+): calcd 290.1406, found 290.1410.

(2-Chloro-6-methylphenyl)(8-methoxy-imidazo[1,5-*a*]-quinoxalin-4-yl)amine (21). Compound **21** was prepared according to a procedure described in the literature.[28,29] Mp: 202−204 °C. ^{1}H NMR (400 MHz, DMSO-d_6): δ 9.30 (bs, 1H), 9.10 (s, 1H), 8.11 (d, J = 8.86 Hz, 1H), 7.44 (d, J = 7.49 Hz, 1H), 7.25−7.38 (m, 2H), 6.87 (d, J = 8.86 Hz, 1H), 6.83 (s, 1H), 3.77 (s, 3H), 2.24 (s, 3H).

***N*-(2-Chloro-6-methylphenyl)-2-methoxyimidazo[1,5-*a*]-pyrido[3,2-*e*]pyrazin-6-amine (22a).** Compound **22a** was prepared from **12** by a route analogous to that used for the preparation of **20**. Mp: 261−262 °C. ^{1}H NMR (400 MHz, DMSO-d_6): δ 9.32 (s, 1H), 8.98 (s, 1H), 8.03 (bs, 1H), 7.76 (d, J = 8.70 Hz, 1H), 7.43 (m, 1H), 7.27−7.35 (m, 2H), 6.87 (d, J = 8.70 Hz, 1H), 4.00 (s, 3H), 2.25 (s, 3H). MS (ESI): m/z = 340$^+$ (M + 1). HR-MS (ESI-TDF) for $C_{17}H_{15}ClN_5O$ (MH^+): calcd 340.0965, found 340.0965.

***N*^{6}-(2-Chloro-6-methylphenyl)-*N*^{2},*N*^{2}-dimethylimidazo-[1,5-*a*]pyrido[3,2-*e*]pyrazine-2,6-diamine (22b).** Compound **22b** (>30 mg) was prepared in >80% yield from **12** (30 mg) by a route analogous to that used for the preparation of **4**. ^{1}H NMR (400 MHz, DMSO-d_6): δ 9.07 (bs, 1H), 8.95 (s, 1H), 8.01 (bs, 1H), 7.64 (d, J = 9.00 Hz, 1H), 7.48 (m, 1H), 7.30−7.47 (m, 2H), 6.80 (d, J = 9.00 Hz, 1H), 3.18 (s, 6H), 2.30 (s, 3H). MS (ESI): m/z = 353$^+$ (M + 1). HR-MS (ESI-TDF) for $C_{18}H_{17}ClN_6$ (MH^+): calcd 353.1282, found 353.1289.

***N*^{6}-(2-Chloro-6-methylphenyl)-*N*^{2},*N*^{2}-diethylimidazo-[1,5-*a*]pyrido[3,2-*e*]pyrazine-2,6-diamine (22c).** Compound **22c** (>30 mg) was prepared in >80% yield from **12** (30 mg) by a route analogous to that used for the preparation of **4**. ^{1}H NMR (400 MHz, DMSO-d_6): δ 8.98 (bs, 1H), 8.83 (s, 1H), 8.01 (bs, 1H), 7.64 (d, J = 9.05 Hz, 1H), 7.48 (m, 1H), 7.30−7.47 (m, 2H), 6.69 (d, J = 9.05 Hz, 1H), 3.58 (m, 4H), 2.25 (s, 3H), 1.15 (t, J = 6.96 Hz, 6H). MS (ESI): m/z = 381$^+$ (M + 1). HR-MS (ESI-TDF) for $C_{20}H_{22}ClN_6$ (MH^+): calcd 381.1595, found 381.1561.

***N*^{6}-(2-Chloro-6-methylphenyl)-*N*^{2}-[2-(dimethylamino-ethyl)]-*N*^{2}-methylimidazo[1,5-*a*]pyrido[3,2-*e*]pyrazine-2,6-diamine (22d).** Compound **22d** (>30 mg) was prepared in >80% yield from **12** (30 mg) by a route analogous to that used for the preparation of **4**. ^{1}H NMR (400 MHz, $CDCl_3$): δ 8.80 (s, 1H), 7.70 (d, J = 8.87 Hz, 1H), 7.34 (m, 1H), 7.18−7.24 (m, 3H), 6.62 (d, J = 8.87 Hz, 1H), 6.45 (bs, 1H), 3.78 (t, J = 7.28 Hz, 2H), 3.15 (s, 3H), 2.58 (t, J = 7.28 Hz, 1H), 2.34 (s, 6H), 2.32 (s, 3H).

***N*-(2-Chloro-6-methylphenyl)-2-(4-morpholino)imidazo-[1,5-*a*]pyrido[3,2-*e*]pyrazin-6-amine (22f).** Compound **22f** (>30 mg) was prepared in >80% yield from **12** (30 mg) by a route analogous to that used for the preparation of **4**. Mp: 222−224 °C. ^{1}H NMR (400 MHz, DMSO-d_6): δ 9.12 (bs, 1H), 8.95 (s, 1H), 7.97 (bs, 1H), 7.63 (d, J = 8.95 Hz, 1H), 7.43 (d, J = 7.87 Hz, 1H), 7.25−7.33 (m, 2H), 6.93 (d, J = 8.95 Hz,

1H), 3.74 (m, 4H), 3.56 (m, 4H), 2.24 (s, 3H). MS (ESI): m/z = 395$^+$ (M + 1). HR-MS (ESI-TDF) for $C_{20}H_{20}ClN_6O$ (MH^+): calcd 395.1387, found 395.1392.

***N*-(2-Chloro-6-methylphenyl)-2-(1-piperidinyl)imidazo-[1,5-*a*]pyrido[3,2-*e*]pyrazin-6-amine (22g).** Compound **22g** (>30 mg) was prepared in >80% yield from **12** (30 mg) by a route analogous to that used for the preparation of **4**. Mp: 257−259 °C. ^{1}H NMR (400 MHz, DMSO-d_6): δ 8.93 (bs, 1H), 8.79 (s, 1H), 7.84 (bs, 1H), 7.46 (d, J = 8.98 Hz, 1H), 7.31 (d, J = 7.70 Hz, 1H), 7.13−7.22 (m, 2H), 6.79 (d, J = 8.98 Hz, 1H), 3.46−3.57 (m, 4H), 1.40−1.60 (m, 6H). MS (ESI): m/z = 393$^+$ (M + 1). HR-MS (ESI-TDF) for $C_{21}H_{22}ClN_7$ (MH^+): calcd 393.1595, found 393.1592.

***N*-(2-Chloro-6-methylphenyl)-2-(1-piperazinyl)imidazo-[1,5-*a*]pyrido[3,2-*e*]pyrazin-6-amine (22h).** Compound **22h** (>30 mg) was prepared in >80% yield from **12** (30 mg) by a route analogous to that used for the preparation of **4**. Mp: 191−193 °C. ^{1}H NMR (400 MHz, DMSO-d_6): δ 8.91 (bs, 1H), 8.74 (s, 1H), 7.78 (bs, 1H), 7.42 (d, J = 8.82 Hz, 1H), 7.24 (dd, J = 6.65 Hz, J = 1.09 Hz, 1H), 7.15 (d, J = 6.65 Hz, 1H), 7.10 (dd, AB pattern, J = 7.66 Hz, $\Delta\nu$ = 14.15, 1H), 6.72 (d, J = 8.92 Hz, 1H), 3.34−3.37 (m, 4H), 2.64−2.67 (m, 4H), 2.07 (s, 3H). MS (ESI): m/z = 394$^+$ (M + 1). HR-MS (ESI-TDF) for $C_{20}H_{21}ClN_7$ (MH^+): calcd 394.1547, found 394.1552.

***N*-(2-Chloro-6-methylphenyl)-2-(4-methyl-1-piperazi-nyl)imidazo[1,5-*a*]pyrido[3,2-*e*]pyrazin-6-amine (22i).** Compound **22i** (>30 mg) was prepared in >80% yield from **12** (30 mg) by a route analogous to that used for the preparation of **4**. Mp: 232−233 °C. ^{1}H NMR (400 MHz, DMSO-d_6): δ 9.15 (s, 1H), 8.99 (s, 1H), 8.02 (bs, 1H), 7.66 (d, J = 8.97 Hz, 1H), 7.48 (d, J = 7.57 Hz, 1H), 7.31−7.39 (m, 2H), 6.98 (d, J = 8.97 Hz, 1H), 3.65 (m, 4H), 2.56 (s, 3H), 2.49 (m, 4H), 2.29 (s, 3H). MS (ESI): m/z = 408$^+$ (M + 1). HR-MS (ESI-TDF) for $C_{21}H_{23}ClN_7$ (MH^+): calcd 408.1703, found 408.1693.

***N*-(2-Chloro-6-methylphenyl)-2-(hexahydro-1*H*-1,4-di-azepin-1-yl)imidazo[1,5-*a*]pyrido[3,2-*e*]pyrazin-6-amine (22j).** Compound **22j** (>30 mg) was prepared in >80% yield from **12** (30 mg) by a route analogous to that used for the preparation of **4**. Mp: 148−149 °C. ^{1}H NMR (400 MHz, DMSO-d_6): δ 8.92 (bs, 1H), 8.80 (s, 1H), 7.87 (s, 1H), 7.49 (d, J = 8.97 Hz, 1H), 7.35 (dd, J = 7.72 Hz, J = 1.03 Hz, 1H), 7.25 (d, J = 7.72 Hz, 1H), 7.21 (dd, AB pattern, J = 7.72 Hz, $\Delta\nu$ = 14.51, 1H), 6.67 (d, J = 8.97 Hz, 1H), 3.70 (m, 2H), 3.66 (m, 2H), 2.82 (m, 2H), 2.58 (m, 2H), 2.18 (s, 3H), 1.78 (m, 2H). MS (ESI): m/z = 408$^+$ (M + 1). HR-MS (ESI-TDF) for $C_{21}H_{23}ClN_7$ (MH^+): calcd 408.1704, found 408.1717.

***N*-(2-Chloro-6-methylphenyl)-2-(3,5-dimethyl-1-piper-azinyl)imidazo[1,5-*a*]pyrido[3,2-*e*]pyrazin-6-amine (22k).** Compound **22k** (>30 mg) was prepared in >80% yield from **12** (30 mg) by a route analogous to that used for the preparation of **4**. Mp:249−251 °C. ^{1}H NMR (400 MHz, DMSO-d_6): δ 8.83 (s, 1H), 7.72 (d, J = 8.92 Hz, 1H), 7.35 (dd, J = 1.86 Hz, J = 7.46 Hz, 1H), 7.18−7.24 (m, 3H), 6.77 (d, J = 8.92 Hz, 1H), 6.58 (bs, 1H), 4.25 (dd, J = 2.23 Hz, J = 12.54 Hz, 2H), 2.99 (m, 2H), 2.51 (t, J = 12.54 Hz, 2H), 2.32 (s, 3H), 1.21 (s, 3H), 1.19 (s, 3H). MS (ESI): m/z = 422$^+$ (M + 1). HR-MS (ESI-TDF) for $C_{22}H_{25}ClN_7$ (MH^+): calcd 422.1860, found 422.1863.

***N*-(2-Chloro-6-methylphenyl)-8-(3,5-dimethyl-1-piper-azinyl)imidazo[1,5-*a*]pyrido[3,4-*e*]pyrazin-6-amine (23).** Compound **23** was prepared from 4,6-dichloro-3-pyridine carboxylic acid[65] or 2-chloro-4-amino-5-nitropyridine[66] by a route analogous to that used for the preparation of **4**. ^{1}H NMR (400 MHz, DMSO-d_6): δ 9.31 (s, 1H), 9.15 (bs, 1H), 8.26 (bs, 1H), 8.05 (s, 1H), 7.54 (s, 1H), 7.49 (d, J = 7.74 Hz, 1H), 7.39 (d, J = 6.60 Hz, 1H), 7.35 (d, J = 7.64 Hz, 1H), 7.32 (d, J = 7.64 Hz, 1H), 4.27 (d, J = 12.04 Hz, 2H), 2.86 (m, 2H), 2.35 (m, 2H), 2.30 (s, 3H), 1.13 (s, 3H), 1.12 (s, 3H).

(*R*)-1-[6-[(2-Chloro-6-methylphenyl)amino]imidazo[1,5-*a*]pyrido[3,2-*e*]pyrazine-2-]-3-pyrrolidinol (25). Compound **25** (>30 mg) was prepared in >80% yield from **12** (30 mg) using a method analogous to the preparation of **4**. ^{1}H NMR (400 MHz, DMSO-d_6): δ 8.99 (s, 1H), 8.84 (bs, 1H), 7.95 (bs, 1H), 7.58 (d, J = 8.82 Hz, 1H), 7.42 (d, J = 7.72 Hz, 1H), 7.31 (d, J = 6.90 Hz, 1H), 7.29 (d, J = 7.72 Hz, 1H), 7.25 (d, J = 7.72 Hz, 1H), 6.55 (d, J = 8.82 Hz, 1H), 5.00 (bs, 1H), 4.42 (bs, 1H),3.50−3.63 (m, 3H), 3.42 (m, 1H), 2.24 (s, 3H), 2.05 (m, 1H), 1.94 (m, 1H).

(*S*)-1-[6-[(2-Chloro-6-methylphenyl)amino]imidazo[1,5-*a*]pyrido[3,2-*e*]pyrazine-2-]-3-pyrrolidinol (26). Compound **25** (>30 mg) was prepared in >80% yield from **12** (30 mg) using a method analogous to the preparation of **4**. ^{1}H NMR (400 MHz, DMSO-d_6): δ 8.99 (s, 1H), 8.84 (bs, 1H), 7.95 (bs, 1H), 7.58 (d, J = 8.82 Hz, 1H), 7.42 (d, J = 7.72 Hz, 1H), 7.31 (d, J = 6.90 Hz, 1H), 7.29 (d, J = 7.72 Hz, 1H), 7.25 (d, J = 7.72 Hz, 1H), 6.55 (d, J = 8.82 Hz, 1H), 5.00 (bs, 1H), 4.42 (bs, 1H),3.50−3.63 (m, 3H), 3.42 (m, 1H), 2.24 (s, 3H), 2.05 (m, 1H), 1.94 (m, 1H).

(*S*)-2-(3-Amino-1-pyrrolidinyl)-*N*-(2-chloro-6-methylphen-yl)imidazo[1,5-*a*]pyrido[3,2-e]pyrazin-6-amine (29). Compound **29** (>30 mg) was prepared in >80% yield from **12** (30 mg) using a method analogous to the preparation of **4**. ^{1}H NMR (400 MHz, DMSO-d_6): δ 9.10 (bs, 1H), 8.90 (s, 1H), 8.03 (bs, 1H), 7.67 (d, J = 8.78 Hz, 1H), 7.48 (d, J = 7.88 Hz, 1H), 7.38 (d, J = 6.92 Hz, 1H), 7.36 (d, J = 7.64 Hz, 1H), 7.32 (d, J = 7.64 Hz, 1H), 3.42−3.92 (m, 5H), 2.30 (s, 3H), 2.29 (m, 1H), 2.04 (m, 1H).

(*R*)-2-(3-Amino-1-pyrrolidinyl)-*N*-(2-chloro-6-methylphen-yl)imidazo[1,5-*a*]pyrido[3,2-*e*]pyrazin-6-amine (30). Compound **30** (>30 mg) was prepared in >80% yield from **12** (30 mg) using a method analogous to the preparation of **4**. ^{1}H NMR (400 MHz, DMSO-d_6): δ 9.10 (bs, 1H), 8.90 (s, 1H), 8.03 (bs, 1H), 7.67 (d, J = 8.78 Hz, 1H), 7.48 (d, J = 7.88 Hz, 1H), 7.38 (d, J = 6.92 Hz, 1H), 7.36 (d, J = 7.64 Hz, 1H), 7.32 (d, J = 7.64 Hz, 1H), 3.42−3.92 (m, 5H), 2.30 (s, 3H), 2.29 (m, 1H), 2.04 (m, 1H).

(*R*)-*N*-(2-Chloro-6-methylphenyl)-2-[3-methyl-1-piper-azinyl)imidazo[1,5-*a*]pyrido[3,2-*e*]pyrazin-6-amine (31). Compound **31** (>30 mg) was prepared in >80% yield from **12** (30 mg) using a method analogous to the preparation of **4**. Mp: 162−164 °C. ^{1}H NMR (400 MHz, DMSO-d_6): δ 9.00 (bs, 1H), 8.87 (s, 1H), 7.89 (bs, 1H), 7.52 (d, J = 8.98 Hz, 1H), 7.36 (dd, J = 1.22 Hz, 1H), 7.18−7.26 (m, 2H), 6.83 (d, J = 8.98 Hz, 1H), 4.17 (m, 2H), 2.90 (m, 1H), 2.58−2.75 (m, 3H), 2.34 (m, 1H), 2.22 (m, 1H), 2.17 (s, 1H), 0.99 (d, J = 6.26 Hz, 3H). MS (ESI): m/z = 408$^+$ (M + 1). HR-MS (ESI-TDF) for $C_{21}H_{22}ClN_7$ (MH^+): calcd 408.1703, found 408.1706.

(*R*)-4-[6-[(2-Chloro-6-methylphenyl)amino]imidazo[1,5-*a*]pyrido[3,2-*e*]pyrazin-2-yl]-2-piperazine Methanol (32). Compound **32** (>30 mg) was prepared in >80% yield from **12** (30 mg) using a method analogous to the preparation of **4**. Mp: 177−179 °C. ^{1}H NMR (400 MHz, DMSO-d_6): δ 8.99 (bs, 1H), 8.83 (s, 1H), 7.87 (bs, 1H), 7.51 (d, J = 9.01 Hz, 1H), 7.33 (d, J = 7.71 Hz, 1H), 7.16−7.24 (m, 2H), 6.80 (d, J = 9.01 Hz, 1H), 4.62 (m, 1H), 4.17 (m, 2H), 3.25−3.42 (m, 2H), 2.92 (m, 1H), 2.76 (m, 1H), 2.63 (m, 2H), 2.15 (s, 3H). MS (ESI): m/z = 424$^+$ (M + 1). HR-MS (ESI-TDF) for $C_{21}H_{23}ClN_7O$ (MH^+): calcd 424.1654, found 424.1670.

(*S*)-4-[6-[(2-Chloro-6-methylphenyl)amino]imidazo[1,5-*a*]pyrido[3,2-*e*]pyrazin-2-yl]-2-piperazine Methanol (33). Compound **33** (>30 mg) was prepared in >80% yield from **12** (30 mg) using a method analogous to the preparation of **4**. Mp: 182−184 °C. ^{1}H NMR (400 MHz, DMSO-d_6): δ 8.99 (bs, 1H), 8.83 (s, 1H), 7.87 (bs, 1H), 7.51 (d, J = 9.01 Hz, 1H), 7.33 (d, J = 7.71 Hz, 1H), 7.16−7.24 (m, 2H), 6.80 (d, J = 9.01 Hz, 1H), 4.62 (m, 1H), 4.17 (m, 2H), 3.25−3.42 (m, 2H), 2.92 (m, 1H), 2.76 (m, 1H), 2.63 (m, 2H), 2.15 (s, 3H). MS (ESI): m/z = 424$^+$ (M + 1). HR-MS (ESI-TDF) for $C_{21}H_{23}ClN_7O$ (MH^+): calcd 424.1654, found 424.1659.

4-[6-[2-Chloro-6-methylphenyl)amino]imidazo[1,5-*a*]-pyrido[3,2-*e*]pyrazin-2-yl]-1-piperazine Ethanol (34). Compound **34** (>30 mg) was prepared in >80% yield from **12** (30 mg) using a method analogous to the preparation of **4**. Mp: 235.5−236.5 °C. ^{1}H NMR (400 MHz, DMSO-d_6): δ 9.01 (bs, 1H), 8.86 (s, 1H), 7.89 (bs, 1H), 7.53 (d, J = 8.97 Hz, 1H), 7.35 (dd, J = 7.84 Hz, J = 1.22 Hz, 1H), 7.25 (d, J = 7.76 Hz, 1H), 7.21 (dd, J = 7.76 Hz, $\Delta\nu$ = 13.99, 1H), 6.84 (d, J = 8.97 Hz, 1H), 4.38 (t, J = 5.34 Hz, 1H), 3.46−3.53 (m, 6H), 2.47 (m, 4H), 2.37 (m, 2H), 2.16 (s, 3H). MS (ESI): m/z = 438$^+$ (M +

1). HR-MS (ESI-TDF) for $C_{22}H_{25}N_7ClO$ (MH^+): calcd 438.1809, found 438.1812.

***N*-(2-Chloro-6-methylphenyl)-2-[4-[2-(dimethylamino)-ethyl]-1-piperazinyl]imidazo[1,5-*a*]pyrido[3,2-*e*]pyrazin-6-amine (35).** Compound **35** (>30 mg) was prepared in >80% yield from **12** (30 mg) using a method analogous to the preparation of **4**. Mp: 177−179 °C. ^{1}H NMR (400 MHz, DMSO-d_6): δ 9.01 (bs, 1H), 8.86 (s, 1H), 7.89 (bs, 1H), 7.53 (d, J = 8.97 Hz, 1H), 7.36 (dd, J = 7.84 Hz, J = 1.22 Hz, 1H), 7.25 (d, J = 7.76 Hz, 1H), 7.20 (dd, J = 7.76 Hz, $\Delta\nu$ = 13.99, 1H), 6.84 (d, J = 8.97 Hz, 1H), 3.51 (m, 4H), 2.40−2.50 (m, 4H), 2.32−2.37 (m, 4H), 2.16 (s, 3H), 2.09 (s, 6H). MS (ESI): m/z = 465$^+$ (M + 1). HR-MS (ESI-TDF) for $C_{24}H_{30}ClN_8$ (MH^+): calcd 465.2282, found 465.2286.

(*R*)-3-[[6-[(2-Chloro-6-methylphenyl)amino]imidazo-[1,5-*a*]pyrido[3,2-*e*]pyrazin-2-yl]methylamino]-1,2-propanediol (37). Compound **37** (>30 mg) was prepared in >80% yield from **12** (30 mg) using a method analogous to the preparation of **4**. Mp: 187−189 °C. ^{1}H NMR (400 MHz, DMSO-d_6): δ 8.84 (bs, 1H), 8.72 (s, 1H), 7.79 (bs, 1H), 7.41 (d, J = 8.92 Hz, 1H), 7.26 (d, J = 7.69 Hz, 1H), 7.16 (d, J = 6.75 Hz, 1H), 7.11 (dd, J = 7.69 Hz, 1H, $\Delta\nu$ = 14.32, 1H), 6.57 (d, J = 8.92 Hz, 1H), 4.63 (d, J = 6.07 Hz, 1H), 4.51 (t, J = 5.61 Hz, 1H), 3.60−3.70 (m, 2H), 3.20 (m, 3H), 3.00 (s, 3H), 2.08 (s, 3H). MS (ESI): m/z = 413$^+$ (M + 1). HR-MS (ESI-TDF) for $C_{20}H_{22}ClN_6O_2$ (MH^+): calcd 413.1493, found 413.1497.

(*S*)-3-[[6-[(2-Chloro-6-methylphenyl)amino]imidazo-[1,5-*a*]pyrido[3,2-*e*]pyrazin-2-yl]methylamino]-1,2-propanediol (38). Compound **38** (>30 mg) was prepared in >80% yield from **12** (30 mg) using a method analogous to the preparation of **4**. Mp: 190−192 °C. ^{1}H NMR (400 MHz, DMSO-d_6): δ 8.84 (bs, 1H), 8.72 (s, 1H), 7.79 (bs, 1H), 7.41 (d, J = 8.92 Hz, 1H), 7.26 (d, J = 7.69 Hz, 1H), 7.16 (d, J = 6.75 Hz, 1H), 7.11 (dd, J = 7.69 Hz, $\Delta\nu$ = 14.32, 1H), 6.57 (d, J = 8.92 Hz, 1H), 4.63 (d, J = 6.07 Hz, 1H), 4.51 (t, J = 5.61 Hz, 1H), 3.60−3.70 (m, 2H), 3.20 (m, 3H), 3.00 (s, 3H), 2.08 (s, 3H). MS (ESI): m/z = 413$^+$ (M + 1). HR-MS (ESI-TDF) for $C_{20}H_{22}ClN_6O_2$ (MH^+): calcd 413.1493, found 413.1496.

2-[[6-(2-Chloro-6-methylphenyl)amino]imidazo[1,5-*a*]-pyrido[3,2-*e*]pyrazin-2-yl]methylamino]ethanol (39). Compound **39** (>30 mg) was prepared in >80% yield from **12** (30 mg) using a method analogous to the preparation of **4**. Mp: 195−197 °C. ^{1}H NMR (400 MHz, $CDCl_3$): δ 8.78 (s, 1H), 7.73 (d, J = 8.96 Hz, 1H), 7.35 (m, 1H), 7.18−7.24 (m, 3H), 7.67 (d, J = 8.96 Hz, 1H), 3.96 (m, 2H), 3.85 (m, 2H), 3.19 (s, 3H), 3.00 (bs, 1H), 2.32 (s, 3H).

2-[[6-(2-Chloro-6-methylphenyl)amino]imidazo[1,5-*a*]-pyrido[3,2-*e*]pyrazin-2-yl]amino]ethanol (40). Compound **40** (>30 mg) was prepared in >80% yield from **12** (30 mg) using a method analogous to the preparation of **4**. Mp: 259−261 °C. ^{1}H NMR (400 MHz, DMSO-d_6): δ 8.88 (bs, 1H), 8.75 (s, 1H), 7.85 (bs, 1H). 7.39 (d, J = 8.76 Hz, 1H), 7.36 (d, J = 7.68 Hz, 1H), 7.26 (d, J = 6.75 Hz, 1H), 7.18 (dd, J = 7.68 Hz, $\Delta\nu$ = 14.48, 1H), 6.87 (m, 1H), 6.54 (d, J = 8.76 Hz, 1H), 4.70 (bs, 1H), 3.54 (m, 2H), 3.40 (m, 2H), 2.17 (s, 3H). MS (ESI): m/z = 369$^+$ (M + 1). HR-MS (ESI-TDF) for $C_{18}H_{18}N_6ClO$ (MH^+): calcd 369.1230, found 369.1236.

Lck Enzyme Assay. Recombinant Lck expressed as a His-tagged protein in insect cells using a baculovirus expression system and purified by nickel affinity chromatography is incubated in kinase buffer (20 mM MOPS, pH7, 10 mM $MgCl_2$) in the presence of the test compound. The reaction was initiated by the addition of substrates to the final concentration of 1 μM ATP, 3.3 μCi/mL [^{33}P] g-ATP, and 0.1 mg/mL acid denatured enolase, and was stopped after 10 min by the addition of 10% trichloroacetic acid, 100 mM sodium pyrophosphate followed by 2 mg/mL bovine serum albumin. The labeled enolase protein substrate was precipitated at 4 °C, harvested onto Packard Unifilter plates, and counted in a Topcount scintillation counter.

T Cell (Human PBL) Proliferation Assay. A 96-well plate was coated with a monoclonal antibody to CD3 (G19-4), the antibody was allowed to bind, and the plate was washed. Normal human peripheral blood T cells were added to the wells along with test compound plus anti-CD28 (E.3) antibody. After 3 days, the [^{3}H]-thymidine was added to the cells, and after further incubation, the cells were harvested and counted in a scintillation counter.

Inhibition of Serum Interleukin-2 (IL-2) in Mouse. BALB/c female mice, 8−10 weeks of age (Harlan Teklad, Indianapolis, IN), were dosed by oral gavage (po) with either vehicle alone (propylene glycol−water, 50:50, v/v) or compound **4** dissolved in vehicle, or cyclosporin A (CsA, Neoral; Novartis, East Hanover, NJ). One hour later, mice were injected intravenously (iv) with 500 μg/kg purified anti-CD3 antibody (clone 145-2C11; American Type Culture Collection, Rockville, MD). The mice were bled 1.5 h after anti-CD3 injection. Levels of IL-2 in the serum were determined by ELISA assay according to manufacturer's instructions (R&D Systems, Minneapolis, MN).

Inhibition of Serum Tumor Necrosis Factor α (TNFα) in Mouse. C57BL/6 female mice, 8−10 weeks of age (Harlan Teklad, Indianapolis, IN), were dosed by oral gavage (po) with either vehicle alone (propylene glycol−water, 50:50, v/v) or compound **4** dissolved in vehicle. One hour later, mice were injected intravenously (iv) with 500 μg/kg lipopolysaccharide (LPS, *Escherichia coli* 0111:B4; Sigma, St. Louis, MO). Mice were bled 1 h after LPS injection. Levels of TNFα in the serum were determined by ELISA assay according to manufacturer's instructions (R&D Systems, Minneapolis, MN).

Modeling Methods. Lck Model. An initial homology model was developed using the published structure of the Hck−ANP−PNP complex[67] and the Modeler module within Insight.[68] Minor adjustments to the ATP binding site residues were made consistent with observed SAR in the imidazoquinoxaline series, as well as incorporating more recently published Lck structural details.[30]

Multiple Linear Regression. Regression analyses were conducted using the QSAR module within the Cerius2 program.[69] Structures were built within Sybyl[70] and imported into Cerius2 as SD files.

Hydrogen Bond Enthalpy. The potential strength of the hydrogen bond to the imidazolyl nitrogen was determined by modeling a water molecule as a donor (see illustration in Table 6). For each imidazoquinoxaline analogue, three systems were geometry optimized/energy minimized using SAM1:[61] the ligand, the water-complexed ligand, and water. The difference in calculated heats of formation provided an estimate for the hydrogen bond strength in units of kcal/mol.

Acknowledgment. We would like to thank the Discovery Analytical Science Group for analytical support including the high-resolution mass spectra (HR-MS). The authors are grateful for the initial Lck homology model provided by Dr. Donna Bassolino, and the grid-contouring program[71] and helpful suggestions provided by Dr. Andrew Pudzianowski.

References

(1) Isakov, N.; Wange, R. L.; Samolson, L. E. The role of tyrosine kinases and phosphotyrosine-containing recognition motifs in regulation of the T cell-antigen receptor-mediated signal transduction pathway. *J. Leukocyte Biol.* **1994**, *55*, 265−271.

(2) Bolen, J. B.; Brugge, J. S. Leukocyte protein tyrosine kinases: potential targets for drug discovery. *Annu. Rev. Immunol.* **1997**, *15*, 371−404.

(3) Johnson, L. N.; Noble, M. E.; Owen, D. J. Active and inactive protein kinases: structural basis for regulation. *Cell* **1996**, *85* (2), 149−158.

(4) Neumeister, E. N.; Zhu, Y.; Richard, S.; Terhorst, C.; Chan, A. C.; Shaw, A. S. Binding of ZAP-70 to phosphorylated T-cell receptor ζ and η enhances its autophosphorylation and generates specific binding sites for SH2 domain-containing proteins. *Mol. Cell. Biol.* **1995**, *15* (6), 3171−3178.

(5) Chan, A. C.; Dalton, M.; Johnson, R.; Kong, G. H.; Wang, T.; Thoma, R.; Kurosaki, T. Activation of ZAP-70 kinase activity by phosphorylation of tyrosine 493 is required for lymphocyte antigen receptor function. *EMBO J.* **1995**, *14* (11), 2499−2508.

(6) Trobridge, P. A.; Levin, S. D. Lck plays a critical role in Ca^{2+} mobilization and CD28 co-stimulation in mature primary T cells. *Eur. J. Immunol.* **2001**, *31*, 3567−3579.

(7) Kikkawa, U.; Nishizuka, Y. The role of protein kinase C in transmembrane signaling. *A. Rev. Cell. Biol.* **1986**, *2*, 149−178.
(8) Isakov, N.; Mally, M. I.; Scholz, W.; Altman, A. T lymphocyte activation: the role of protein kinase C and the bifurcating inositol phospholipid signal transduction pathway. *Immunol. Rev.* **1987**, *95*, 89−111.
(9) Straus, D. B.; Weiss, A. C. Genetic evidence for the involvement of the Lck tyrosine kinase in signal transduction through the T cell antigen receptor. *Cell* **1992**, *70*, 585−593.
(10) Chan, A. C.; Desia, D. M.; Weiss, A. C., The role of protein tyrosine kinases and protein tyrosine phosphatases in T cell antigen receptor signal transduction. *Annu. Rev. Immunol.* **1994**, *12*, 555−592.
(11) Weiss, A. C.; Littman, D. Signal transduction by lymphocyte antigen receptors. *Cell* **1994**, *76* (2), 263−274.
(12) Hanke, J. H.; Gardner, J. P.; Dow, R. L.; Changelian, P. S.; Brissette, W. H.; Weringer, E. J.; Pollok, B. A. and Connelly, P. A. Discovery of a novel, potent, and Src family-selective tyrosine kinase inhibitor. Study of Lck- and Fyn T-dependent T cell activation. *J. Biol. Chem.* **1996**, *271* (2), 695−701.
(13) Van Oers, N. S. C., Lowin-Kropf, B.; Finlay, D.; Connolly, K.; Weiss, A. T cell development is abolished in mice lacking both Lck and Fyn protein tyrosine kinases. *Immunity* **1996**, *5* (5), 429−436.
(14) Korade-Mirnics, Z.; Corey, S. J. Src kinase-mediated signaling in leukocytes. *J. Leukocyte Biol.* **2000**, *68* (5), 603−613.
(15) Omri, B.;. Blancher, C.; Neron, B.; Marty, M. C.; Rutin, J.; Molina, T. J.; Pessac, B.; Crisanti, P. Retinal dysplasia in mice lacking *p*56^{Lck}. *Oncogene* **1998**, *16* (18), 2351−2356.
(16) Sperber, B. R.; Boyle-Walsh, E. A.; Engleka M. J.; Gadue, P.; Peterson A. C.; Stein P. L.; Scherer S. S.; McMorris, F. A. A unique role for Fyn in CNS myelination. *J. Neurosci.* **2001**, *21* (6), 2039−2047.
(17) Grant, S. G.; O'Dell, T. J.; Karl, K. A.; Stein, P. L.; Soriano, P.; Kandel, E. R. Impaired long-term potentiation, spatial learning, and hippocampal development in Fyn mutant mice. *Science* **1992**, *258* (5090), 1903−1910.
(18) Miyakawa, T.; Yagi, T.; Kitazawa, H.; Yasuda, M.; Kawai, N.; Tsuboi, K.; Niki, H. Fyn-kinase as a determinant of ethanol sensitivity: relation to NMDA-receptor function. *Science* **1997**, *278* (5338), 698−701.
(19) Myers, M. R.; Setzer, N. N.; Spada, A. P.; Zulli, A. L.; Hsu, C.-Y.; Zilberstein, A.; Johnson, S. E.; Hook, L. E.; Jacoski, M. V. The preparation and SAR of 4-(anilino), 4-(phenoxy), and 4-(-(thiophenoxy)quinazolines: inhibitors of p56^{lck} and EGF-R tyrosine kinase activity. *Bioorg. Med. Chem. Lett.* **1997**, *7* (4), 417−420.
(20) Padmanabha, R.; Shu., Y. Z.; Cook, L. S.; Veitch, J. A.; Donovan, M.; Lowe, S.; Huang, S.; Pirnik, D.; Manly, S. P. 1-Methoxy-argoclavine from penicillium sp. WC75209, a novel inhibitor of the Lck tyrosine kinase. *Bioorg. Med. Chem. Lett.* **1998**, *8* (6), 569−574.
(21) Bullington, J. L.; Cameron, J. C.; Davis, J. E.; Dodd, J. H.; Harris, C. A.; Henry, A. R.; Pellegrino-Gensey, J. L.; Rupert, K. C.; Siekierka, J. J. The development of novel and selective p56^{Lck} tyrosine kinase inhibitors. *Bioorg. Med. Chem. Lett.* **1998**, *8* (18), 2489−2494.
(22) Kraker, A. J.; Hartl, B. G.; Amar, A. M.; Bravian, M.; R.; Showalter, H. D. H.; Moore, C. W. Biochemical and cellular effects of *c*-Src kinase-selective pyrido[2,3-d]pyrimidine tyrosine kinase inhibitors. *Biochem. Pharmacol.* **2000**, *60* (7), 885−898.
(23) Goldberg, D. R.; Butz, T.; Cardozo, M. G.; Eckner, R. J.; Hammach, A.; Huang, J.; Jakes, S.; Kapadia, S.; Kashem, M.; Lukas, S.; Morwick, T. M.; Ranzenbeck, M.; Patel, U.; Pav, S.; Peet, G.; Peterson, J. D.; Prokopowicz, A. S.; Snow, R. J.; Sellati, R.; Takahashi, H.; Tan, J.; Tschantz, M. A.; Wang, X.-J, Wang, Y.; Wolak, J.; Xiong, P.; Moss, N. Optimization of 2-phenylaminoimidazo[4,5-*h*]isoquinolin-9-ones: orally active inhibitors of Lck kinase. *J. Med. Chem.* **2003**, *46* (8), 1337−1349.
(24) Arnold, L. D.; Calderwood, D. J.; Dixon, R. W.; Johnston, D. N.; Kamens, J. S.; Munschauer, R.; Rafferty, P.; Ratnofsky, S. E. Pyrrolo[2,3-*d*]pyrimidines containing an extended 5-substituent as potent and selective inhibitors of Lck. *Bioorg. Med. Chem. Lett.* **2000**, *10* (19), 2167−2170.
(25) Burchat, A. F.; Calderwood, D. J.; Hirst, G. C.; Holman, N. J.; Johnston, D. N.; Munschauer, R.; Rafferty, P.; Tometzki, G. B. Pyrrolo[2,3-*d*]pyrimidines containing an extended 5-substituent as potent and selective inhibitors of Lck. *Bioorg. Med. Chem. Lett.* **2000**, *10* (19), 2171−2174.
(26) Hajduk, P. J.; Zhou, M. M.; Fesik, S. W. NMR-based discovery of phosphotyrosine mimetics that bind to the Lck SH2 domain. *Bioorg. Med. Chem. Lett.* **1999**, *9* (16), 2403−2406.
(27) Beaulieu, P. L.; Cameron, D. R.; Ferland, J.-M.; Gauthier J.; Ghiro, E.; Gillard, J.; Gorys, V.; Poirier, M.; Rancourt, J.; Wernic, D.; Llinas-Brunet, M.; Betageri, R.; Cardozo, M.; Hickey, E. R.; Ingraham, R.; Jakes, S.; Kabcenell, A.; Kirrane, T.; Lukas, S.; Patel, U.; Proudfoot, J.; Sharma, R.; Tong, L.; Moss, N. Ligands for the tyrosine kinase p56^{lck} SH2 domain: discovery of potent dipeptide derivatives with monocharged, nonhydrolyzable phosphate replacements. *J. Med. Chem.* **1999**, *42* (10), 1757−1766.
(28) Llinas-Brunet, M.; Beaulieu, P. L.; Cameron, D. R.; Ferland, J.-M.; Gauthier, J.; Ghiro, E.; Gillard, J.; Gorys, V.; Poirier, M.; Rancourt, J.; Wernic, D. Phosphotyrosine-containing dipeptides as high-affinity ligands for the p56^{Lck} SH2 domain. *J. Med. Chem.* **1999**, *42*, 722−729.
(29) Lee, T. R.; Lawrence, D. S. SH2-directed ligands of the Lck tyrosine kinase. *J. Med. Chem.* **2000**, *43* (6), 1173−1179.
(30) Yamaguchi, H.; Hendrickson, W. A. Structural basis for activation of human lymphocyte kinase Lck upon tyrosine phosphorylation. *Nature* **1996**, *384* (5), 484−489.
(31) Zhu, X.; Kim, J. L.; Rose, P. E.; Stover, D. R.; Toledo, L. M.; Zhao, H.; Morgenstern, K. A. Structural analysis of the lymphocyte-specific kinase Lck in complex with non-selective and Src family selective kinase inhibitors. *Structure* **1999**, *7*, 651−661.
(32) Sicheri, F.; Kuriyan, J. Structures of Src-family tyrosine kinases. *Curr. Opin. Struct. Biol.* **1997**, *7*, 777−785.
(33) Chen, P.; Norris, D.; Iwanowicz, E. J.; Spergel, S. H.; Lin, L.; Gu, H. H.; Shen, Z.; Wityak, J.; Lin, T.; Pang, S.; de Fex, H. F.; Pitt, S.; Shen, D. R.; Doweyko, A. M.; Bassolino, D. A.; Roberge, J. Y.; Poss, M. A.; Chen, B.-C.; Schieven, G. L.; Barrish, J. C. Discovery and initial SAR of imidazoquinoxalines as inhibitors of the Src-family kinase p56^{Lck}. *Bioorg. Med. Chem. Lett.* **2002**, *12*, 1361−1364.
(34) Palmer, B. D.; Trumpp-Kallmeyer, S.; Fry, D. W.; Nelson, J. M.; Showalter, H. H. D.; Denny, W. A. Tyrosine kinase inhibitors. 11. Soluble analogues of pyrrolo- and pyrazoloquinazolines as epidermal growth factor receptor inhibitors: synthesis, biological evaluation, and modeling of the mode of binding. *J. Med. Chem.* **1997**, *40* (10), 1519−1529.
(35) Thompson, A. M.; Murray, D. K.; Elliott, W. L.; Fry, D. W.; Nelson, J. A.; Showalter, H. D. H.; Roberts, B. J.; Vincent, P. W.; Denny, W. A. Tyrosine kinase inhibitors. 13. Structure−activity relationships for soluble 7-substituted 4-[(3-bromophenyl)amino]pyrido[4,3-*d*]pyrimidines designed as inhibitors of the tyrosine kinase activity of the epidermal growth factor receptor. *J. Med. Chem.* **1997**, *40* (24), 3915−3925.
(36) Rewcastle, G. W.; Murray, D. K.; Elliott, W. L.; Fry, D. W.; Howard, C. T.; Nelson, J. M.; Roberts, B. J.; Vincent, P. W.; Showalter, H. D. H.; Winters, R. T.; Denny, W. A. Tyrosine kinase inhibitors. 14. Structure−activity relationships for methylamino-substituted derivatives of 4-[(3-bromophenyl)amino]-6-(methylamino)pyrido[3,4-*d*]pyrimidine (PD 158780), a potent and specific inhibitor of the tyrosine kinase activity of receptors for the EGF family of growth factors. *J. Med. Chem.* **1998**, *41* (5), 742−751.
(37) Hennequin, L. F.; Stokes, E. S.; Thomas, A. P.; Johnstone, C.; Ple, P. A.; Ogilvie, D. J.; Dukes, M.; Wedge, S. R.; Kendrew, J.; Curwen, J. O. Novel 4-anilonoquinazolines with C-7 basic side chains: design and structure activity relationship of a series of potent, orally active, VEGF receptor tyrosine kinase inhibitors. *J. Med. Chem.* **2002**, *45* (6), 1300−1312.
(38) Chen, P.; Iwanowicz, E. J.; Norris, D.; Gu, H. H.; Lin, L.; Moquin, R. V.; Das, J.; Wityak, J.; Spergel, S. H.; de Fex, H.; Pang, S.; Pitt, S.; Shen, D. R.; Schieven, G. L.; Barrish, J. C. Synthesis and SAR of novel imidazoquinoxaline-based Lck inhibitors: improvement of cell potency. *Bioorg. Med. Chem. Lett.* **2002**, *12*, 3153−3156.
(39) Norris, D.; Chen, P.; Barrish, J. C.; Das, J.; Moquin, R.; Chen, B.-C.; Guo, P. Synthesis of imidazo[1,5-*a*]quinoxalin-4(5*H*)-one template via a novel intramolecular cyclization process. *Tetrahedron Lett.* **2001**, *42*, 4297−4299.
(40) Additional data of other examples are not shown.
(41) Stefanova, I.; Corcoran, M. L.; Horak, E. M.; Wahl, L. M.; Bolen, J. B.; Horak, I. D.; Lipopolysaccharide induces activation of CD-14 associated protein tyrosine kinase p53/56^{Lyn}. *J. Biol. Chem.* **1993**, *268* (28), 20725−20728.
(42) Ernst, M.; Inglese, M.; Scholz, G. M.; Harder, K. W.; Clay, F. J.; Bozinovski, S.; Waring, P.; Darwiche, R.; Kay, T.; Sly, P.; Collins, R.; Turner, D.; Hibbs, M. L.; Anderson, G. P.; Dunn, A. R. Constitutive activation of the Src family kinase Hck results in spontaneous pulmonary inflammation and an enhanced innate immune response. *J. Exp. Med.* **2002**, *196* (5), 589−604.
(43) English, B. K.; Ihle, J. N.; Myracle, A.; Yi, T. Hck tyrosine kinase activity modulates tumor necrosis factor production by murine macrophages. *J. Exp. Med.* **1993**, *178* (3), 1017−1022.
(44) Odeh, M. New insights into the pathogenesis and treatment of rheumatoid arthritis. *Clin. Immunol. Immunopathol.* **1997**, *83*, 103−106.
(45) Newton, R. C.; Decicco, C. P. Therapeutical potential and strategies for inhibiting tumor necrosis factor-α. *J. Med. Chem.* **1999**, *42*, 2295−2314.

(46) Bertolini, D. R.; Nedwin, G. E.; Bringman, T. S.; Smith, D. D.; Mundy, G. R. Stimulation of bone resorption and inhibition of bone formation in vitro by human tumour necrosis factor. *Nature* **1986**, *319*, 516−518.
(47) Stashenko, P.; Dewhirst, F. E.; Peros, W. J.; Kent, R. L.; Ago, J. M. Synergistic interactions between interleukin-1, tumor necrosis factor, and lymphotoxin in bone resorption. *J. Immunol.* **1987**, *138*, 1464−1468.
(48) Canalis, E. Effects of tumor necrosis factor on bone formation in vitro. *Endocrinology* **1987**, *121*, 1596−1604.
(49) Centrella, M.; McCarthy, T. L.; Canalis, E. Tumor necrosis factor-α inhibits collagen synthesis and alkaline phosphatase activity independently of its effect on deoxyribonucleic acid synthesis in osteoblast-enriched bone cell cultures. *Endocrinology* **1988**, *123*, 1442−1448.
(50) MacNaul, K. L.; Chartrain, N.; Lark, M.; Tocci, M. J.; Hutchinson, N I. Differential effects of IL-1 and TNF-α on the expression of stromelysin, collagenase and their natural inhibitor, TIMP, in rheumatoid human synovial fibroblasts. *Matrix Suppl.* **1992**, *1*, 198−199.
(51) Ahmadzadeh, N.; Shingu, M.; Nobunago, M. The effect of recombinant tumor necrosis factor-α on superoxide and metalloproteinase production by synovial cells and chondrocytes. *Clin. Exp. Rheumatol.* **1990**, *8*, 387−391.
(52) Elliott, M. J.; Maini, R. N.; Feldman, M. Treatment of rheumatoid arthritis with chimeric monoclonal antibodies to tumor necrosis factor α. *Arthritis Rheum.* **1993**, *36*, 1681−1690.
(53) Elliott, M. J.; Maini, R. N.; Feldman, M. Randomised double-blinded comparison of chemeric monoclonal antibodies to tumor necrosis factor α (cA2) versus placebo in rheumatoid arthritis. *Lancet* **1994**, *344*, 1105−1110.
(54) Elliott, N. J.; Maini, R. N.; Feldman, M. Repeated therapy with monoclonal antibody to tumour necrosis factor α (cA2) in patients with rheumatoid arthritis. *Lancet* **1994**, *344*, 1125−1127.
(55) Lorenz. H.-M.; Antoni, C.; Valerius, T.: Repp, R.; Grunke, M.; Schweredtner, N.; Nublein, H.; Woody, J.; Kalden, J. R.; Manger, B. *In vivo* blockade of TNF-α by intravenous infusion of a chimeric monoclonal TNF-α antibody in patients with rheumatoid arthritis: short term cellular and molecular effects. *J. Immunol.* **1996**, *156*, 1646−1653.
(56) Moreland, L. W.; Baumgartner, S. W.; Schiff, M. H.; Tindall, E. A.; Fleischmann, R. M.; Weaver, A. L.; Ettlinger, R. E.; Cohen, S.; Koopman, W. J.; Mohler, K.; Widmer, M. B.; Blosch, C. M. Treatment of rheumatoid arthritis with a recombinant human tumor necrosis factor receptor (p75)-Fc fusion protein. *New Engl. J. Med.* **1997**, *337*, 141−147.
(57) Lipsky, P. E.; van der Heijde, D. M. F. M. E.; St. Clair, W.; Furst, D. E.; Breedveld, F. C.; Kalden, J. R.; Smolen, J. S.; Weisman, M.; Emery, P.; Feldmann, M.; Harriman, G. R.; Maini, R. N. Infliximab and methotrexate in the treatment of rheumatoid arthritis. *New Engl. J. Med.* **2000**, *343*, 1594−1602.
(58) Duan, J. J.-W.; Chen, L.; Wasserman, Z. R.; Lu, Z.; Liu, R.-Q.; Covington, M. B.; Qian, M.; Hardman, K. D.; Magolda, R. L.; Newton, R. C.; Christ, D. D.; Wexler, R. R.; Decicco, C. P. Discovery of γ-lactam hydroxamic acids as selective inhibitors of tumor necrosis factor-α converting enzyme: design, synthesis, and structure−activity relationships. *J. Med. Chem.* **2002**, *45*, 4954−4957.
(59) SAM1, semiempirical quantum mechanical program available within AMPAC7 (implemented on SGI/IRIX), Semichem, Inc., Kansas City, MO.
(60) Henry, J. R.; Rupert, K. C.; Dodd, J. H.; Turchi, I. J.; Wadsworth, S. A.; Cavender, D. E.; Fahmy, B.; Olini, G. C.; Davis, J. E.; Pellegrino-Gensey, J. L.; Schafer, P. H.; Siekierka, J. J. 6-Amino-2-(4-fluorophenyl)-4-methoxy-3-(4-pyridyl)-1-H-pyrrolo[2,3-*b*]pyridine (RWF 68354): a potent and selective p38 kinase inhibitor. *J. Med. Chem.* **1998**, *41*, 4196−4198.
(61) Murray, J. S.; Ranganathan, S.; Politzer, P. Correlations between the solvent hydrogen bond acceptor parameter β and the calculated molecular electrostatic potential. *J. Org. Chem.* **1991**, *56*, 3734−3737.
(62) Nikolovska-Coleska, Z.; Suturkova, L.; Dorevski, K.; Krbavcic, A.; Solmajer, T. QSAR of flavonoid inhibitors of p56^{Lck} protein tyrosine kinase: a classical/quantum chemical approach. *QSAR* **1998**, *17*, 7−13.
(63) Huenenberger, P. H.; Helms, V.; Narayana, N.; Taylor, S. McCammon, J. A. Determinants of ligand binding to cAMP-dependent protein kinase. *Biochemistry* **1999**, *38* (8), 2358−2366.
(64) Chen, P.; Barrish, J. C.; Iwanowicz, E.; Lin, J.; Bednarz, M. S.; Chen, B.-C. Reaction of quinoxalin-2-ones with Tos-MIC reagent: synthesis of imidazo[1,5-*a*]quinoxalin-4-ones. *Tetrahedron Lett.* **2001**, *42*, 4293−4295.
(65) Albert, A. and Barlin, G. B. Triazanaphthalenes. Part II. Covalent hydration in 1,4,6-triazanaphthalenes. *J. Chem. Soc.* **1963**, 5156−5166.
(66) Rousseau, R. J.; Robins, R. K. The synthesis of various chloroimidazo[4,5-*c*]pyridines and related derivatives. *J. Heterocycl. Chem.* **1965**, *2* (2), 196−201.
(67) Sicheri, F.; Moarefi, I.; Kuriyan, J. Crystal structure of the Src family tyrosine kinase Hck. *Nature* **1997**, *385*, 602.
(68) InsightII, molecular modeling program for SGI/IRIX workstation, Accelrys, Inc., San Diego, CA.
(69) Cerius2, modeling and simulation program for SGI/IRIX workstation, Accelrys, Inc., San Diego, CA.
(70) Sybyl, molecular modeling program for SGI/IRIX workstation, Tripos, St. Louis, MO.
(71) An in-house implementation of GRID (Goodford, P. *J. Med. Chem.* **1985**, *28*, 849−857) was used as a module within Sybyl.

JM030217E